energies

MDPI

*Review*

# Application of Metal-Organic Frameworks and Covalent Organic Frameworks as (Photo)Active Material in Hybrid Photovoltaic Technologies

**Onur Yildirim [1], Matteo Bonomo [1], Nadia Barbero [1,*], Cesare Atzori [1,2], Bartolomeo Civalleri [1], Francesca Bonino [1], Guido Viscardi [1] and Claudia Barolo [1,3]**

1 Department of Chemistry, NIS Interdepartmental Centre and INSTM Reference Centre, University of Turin, via G. Quarello 15a, 10135 Turin, Italy; onur.yildirim@unito.it (O.Y.); matteo.bonomo@unito.it (M.B.); cesare.atzori@unito.it (C.A.); bartolomeo.civalleri@unito.it (B.C.); francesca.bonino@unito.it (F.B.); guido.viscardi@unito.it (G.V.); claudia.barolo@unito.it (C.B.)

2 European Synchrotron Radiation Facility, 71 Avenue des Martyrs, CS 40220, CEDEX 9, 38043 Grenoble, France

3 ICxT Interdepartmental Centre, Università degli Studi di Torino, Via Lungo Dora, Siena 100, 10153 Turin, Italy

* Correspondence: nadia.barbero@unito.it

Received: 22 September 2020; Accepted: 23 October 2020; Published: 26 October 2020


**Abstract:** Metal-organic frameworks (MOFs) and covalent organic frameworks (COFs) are two innovative classes of porous coordination polymers. MOFs are three-dimensional materials made up of secondary building blocks comprised of metal ions/clusters and organic ligands whereas COFs are 2D or 3D highly porous organic solids made up by light elements (i.e., H, B, C, N, O). Both MOFs and COFs, being highly conjugated scaffolds, are very promising as photoactive materials for applications in photocatalysis and artificial photosynthesis because of their tunable electronic properties, high surface area, remarkable light and thermal stability, easy and relative low-cost synthesis, and structural versatility. These properties make them perfectly suitable for photovoltaic application: throughout this review, we summarize recent advances in the employment of both MOFs and COFs in emerging photovoltaics, namely dye-sensitized solar cells (DSSCs) organic photovoltaic (OPV) and perovskite solar cells (PSCs). MOFs are successfully implemented in DSSCs as photoanodic material or solid-state sensitizers and in PSCs mainly as hole or electron transporting materials. An innovative paradigm, in which the porous conductive polymer acts as standing-alone sensitized photoanode, is exploited too. Conversely, COFs are mostly implemented as photoactive material or as hole transporting material in PSCs.

**Keywords:** metal organic frameworks; covalent organic frameworks; emerging photovoltaics; dye-sensitized solar cells; perovskite solar cells

## 1. Introduction

In the last decades, the demand for sustainable clean energy sources, particularly solar energy, has constantly raised. In spite of the fact that the energy supplied by the Sun's radiation over one year is roughly 10,000 times higher than the world current rate of energy consumption, the state-of-art of the photovoltaic devices are not yet satisfactory because of their low efficiency, high cost and/or limited scale [1].

Nowadays, the most exploited (and efficient) technology for conversion of solar energy to electricity consists in silicon-based devices. In a classical silicon cell, the top and bottom layers are constituted of an *n*-doped and a *p*-doped silicon wafer, in which the charge of the mobile carriers is negative

(electrons) or positive (holes), respectively [2,3]. When the two materials contact each other, electrons and holes transfer over the junction producing an excess of positive charges on one side and an excess of negative charges on the other. The emergent electric field plays then a critical role in the photovoltaic energy conversion process. By absorbing sunlight, electrons are promoted from the valence band to the conduction band of silicon thus generating electron-hole pairs in the materials. The generated electric field collects the photoinduced carriers because it excites the minority carriers over the junction and creates a net photocurrent. As no photocurrent is flowing in the absence of an electric field, the maximum photo-voltage that can be obtained by the device equals the potential difference that is set up in the dark at the *p*–*n* junction that for silicon is about 0.7 V [1]. Photovoltaic based on silicon is an old but still effective technology: the first cell with a sizeable efficiency (5%) was developed by Bell Laboratories in 1953 [4]. The efficiency of the device rapidly increased reaching 14.5% in 1961 when silicon was doped with electron richer or poorer atoms, i.e., phosphorous and boron, respectively. To date, the most efficient single junction device has reached a photoconversion efficiency as high as 29.1% [5]. Better performance could be achieved by coupling various devices to obtain a multijunction solar cell that exceeds the Shockley-Queisser limit [6].

Although silicon-based devices represent the state of art for outdoors use, they fail in indoor applications or in presence of diffuse light. Therefore, in order to resolve this issue, in the last decades scientists have focused their efforts on the so-named "emerging photovoltaics". Among alternative and emerging photovoltaic technologies, dye-sensitized solar cells (DSSCs) and, more recently, perovskite solar cells (PSCs) have gained the greatest attention. As a matter of fact, they couple a scalable, easy and relatively cheap fabrication process to good photoelectrochemical performances and the possibility to be applied in various applications: from indoor [7,8] to portable electronics [9]. More details on these technologies will be given in the following (dedicated) sections.

The development and enhancement in photoconversion of emerging PVs are intimately linked to the improvement of the properties of the constituent materials. In both DSSCs and PSCs a given material can behave as photosensitizer, electrode, electrolyte (in DSSCs) or electron (hole) transport material (in PSCs) [10–12]. Different classes of compounds, e.g., inorganic, [13] organic, [14] metal-organic, [15] could be employed for these different roles.

While such classes of materials have already been thoroughly revised in some recent reviews [16,17], in this context, we aim at reviewing the application of two new classes of materials, namely metal-organic frameworks (MOFs) [18] and covalent organic frameworks (COFs) [19], in hybrid photovoltaic technologies. Both MOFs and COFs belong to the wide family of porous coordination polymers (PCP). Among PCP, MOFs and COFs are becoming more and more attractive (Figure 1). These features can be very interesting for their application in photovoltaics. Indeed, MOFs and COFs crystallinity allows obtaining highly ordered and usually conjugated polymers both in 2D and/or 3D structure. This will give the opportunity to tune the electronic properties of these classes of materials and modify their charge transport ability by slight modification of both metal center (in MOFs) and organic linkers (in both MOFs and COFs). As already stated above, tunability is also fundamental to the different role the frameworks could play in both DSSCs and PSCs [20,21]. For further specification the reader is kindly addressed to the following paragraphs. Both MOFs and COFs usually possess a π-conjugated systems and a wide porous volume that can be tuned with a careful selection of the linker which has strong effects on the structure of the material, especially the electronic one [22,23]. Additionally, COFs show short interlayer distances that could lead to conductive features throughout their structure by organizing an interface between donor and acceptor moieties at a molecular level [19]. MOFs [24–26] and COFs [27,28] are generally synthesized by hydrothermal or solvothermal synthesis and based on condensation reaction. In this method, one of the key roles is played by temperature and solvents mixtures. In particular, in order to favor the synthesis of a crystalline form, solvents should possess different polarities and boiling points [24]. This is of utmost importance as highly crystalline samples are mandatory to apply powerful structural characterization techniques as X-ray or neutron diffraction in order to determine the atomistic structure of the material. While MOFs are synthesized

at a thermodynamical regime where bonds are simultaneously formed and broken, permitting the growth of nice crystals, the same is not true for COFs in which covalent bonds are formed very often in a concerted way. This phenomenon is reasoning the general low crystallinity of COFs, which was tackled by some authors very often with a careful optimization of the synthetic conditions [29,30].

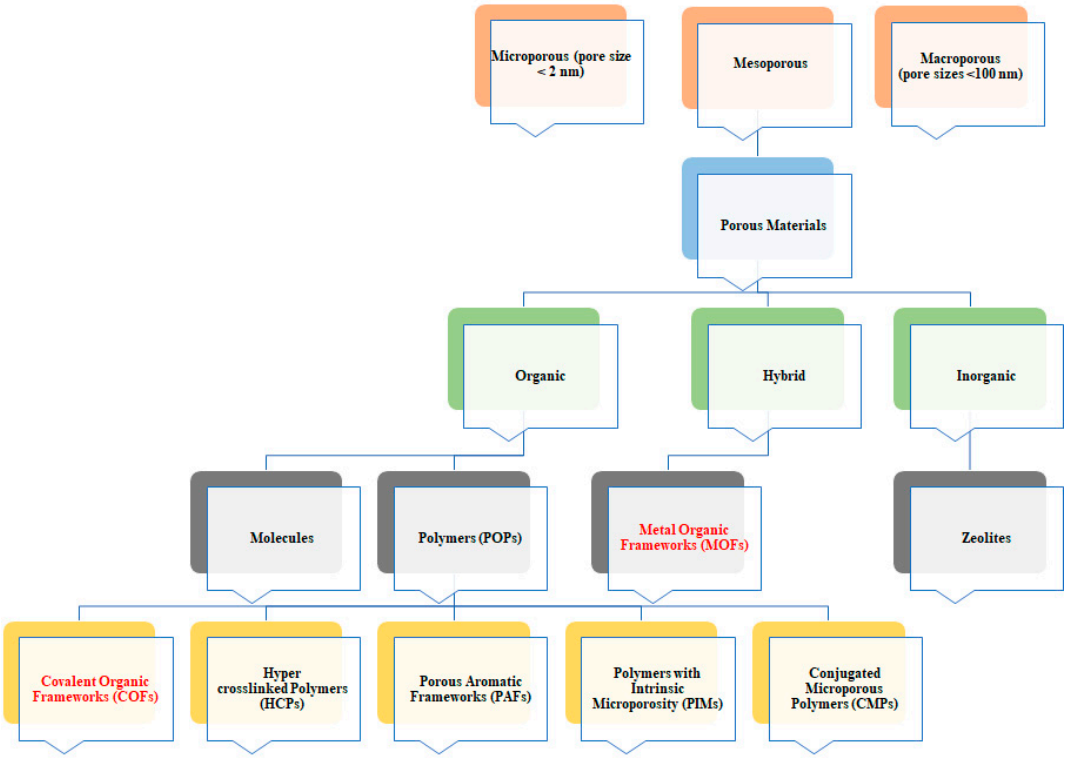


**Figure 1.** Categorization of porous materials based on their pore size and the material varieties.

Although both metal/covalent organic frameworks are generally used for gas storage or catalysis, their optoelectronics and energy storage/conversion properties have been recently explored too [19,31,32]. In this work, we review and critically discuss recent advancement in the application of MOFs and COFs as active materials in emerging photovoltaic technology. It is worth to mention that throughout the present review, we mainly focused our attention on the application of MOFs and COFs in two classes of emerging photovoltaic technology, namely DSSCs and PSCs. With respect to OPV, as far as we are aware, just few examples have been reported in literature; therefore, here, we decided specifically to not tackle this aspect. Indeed, the reader is kindly addressed to some recent reviews for the principle of this technology [33,34]. Theoretically, porous polymers are very promising for this technology being mainly composed by two different organic building blocks, which can exhibit donor and acceptor features and can be used n-type and p-type heterojunction. The first report on COFs in OPVs owed to Prof. T. Bein and Prof. D. Jiang [35–37]. Notwithstanding their promising feature the effective application of this compound is limited by solubility issues affecting the processability of the material itself. This is mainly a drawback when COFs are compared to other porous organic polymers, such as amorphous conjugated microporous polymers (CMPs) or polymers with intrinsic microporosity (PIMs) (Figure 1), that are highly processable [38]. Our analysis is mainly focused on DSSCs and PSCs. As regards organic photovoltaics (OPV), the third family in emerging photovoltaics, just a couple of examples have been reported in literature so far. Therefore, we decided to not specifically tackle this technology in the present review.

### *1.1. Metal-Organic Frameworks (MOFs)*

Metal-organic frameworks are three-dimensional porous coordination polymers made up of secondary building blocks comprised of metal ions/clusters and organic ligands [18,39]. The name metal-organic framework was coined for the first time in 1995 [40]. Afterwards, Cu(II) tricyanomethanide polymeric (crystalline) structures were presented by Biondi et al. [41]. Interestingly, in 1990, a study on the design of scaffold-like materials using Cu(I) centres and tetracyanotetraphenylmethane were reported by Hoskins and Robson [42]. In 1999, Yaghi and his group extended this metal framework to the 3D form by creating a highly porous crystalline structure known as MOF-5 [43]. Later, they also created an isoreticular family of this MOF by employing different carboxylate linkers [44,45].

The synthesis of nanostructures generally takes place through solvothermal methods: commonly, metal precursors and organic linkers are dissolved in solvent and placed in a closed reaction vessel for the construction and self-assembly of MOF crystals. Mostly N,N-dimethylformamide (DMF), N,N-diethylformamide (DEF), methanol, ethanol, and acetonitrile are used as solvents, a temperature lower than 220 °C is usually employed and the crystallization times range from several hours to several days. Recent advances indicate that new synthesis methods such as electrochemical, microwave-assisted, mechanochemical synthesis, microfluidic synthesis methods, etc. have been applied [25]. These different strategies provide some opportunities to control and modify the morphology, size and the chemical functionalization of crystals that impact on properties and performances of the obtained MOF materials [46].

Up to now, more than 70,000 different MOF structures have been reported [47] with surface area values ranging from 1000 to 10,000 $m^2/g$. This exceeds by far those of common porous materials such as zeolites and carbons [48]. Concerning applications, MOFs were firstly employed as catalysts for the first time in 1994 to promote the cyanosilylation of aldehydes [49] and as hydrogen adsorption materials later in 2003 [50]. They are very promising for applications as (photo)active materials in photocatalysis and artificial photosynthesis because of their tunable electronic properties, their structural versatility, and their easy and relative low-cost synthesis [23,51–54]. Furthermore, embodiment of photoactive ligands into MOFs represents an attractive and unconventional approach to study energy transfer, light harvesting, and photo-excited reactivity within well-ordered and properly designed architecture [18,32,55–59]. Remarkably, MOFs have been also employed to improve the stability of conventional solar cells as the ones based on $Cu_2S$/CdS. For instance, Nevruzoglu et al. adopted MOFs as a source of copper to minimize the performance degradation caused by the rapid diffusion of Cu ions into the CdS layer. Alternatively, zirconium-based MOFs could be implemented owing to their high thermal and chemical stabilities [60,61].

### *1.2. Covalent Organic Frameworks (COFs)*

Covalent organic frameworks (COFs) are a class of crystalline porous organic polymers with permanent porosity and highly ordered structures. COFs possess unique conformations and morphologies generating a confined molecular space and interface that interacts with photons, electrons, holes, spins, ions, and molecules, creating new molecular platforms for structural design and functional development [27].

Self-assemblies of molecular COFs layers have recently gained attention as a feasible class of semiconducting polymers [19]. The full organic nature of COFs allows to obtain highly tunable structures that could be easily functionalized with both acceptor or donor groups. Straightforwardly, COFs are starting to be implemented as conductive polymers in photovoltaic applications. COFs are generally constituted by two different organic linkers, that could have a ditopic (C2, two active functional groups), tritopic (C3, three active functional groups) or tetratopic (C4, four active functional groups) geometry leading to 2D or 3D materials. Figure S1A shows different monomers that can be employed to obtain 2D COFs: indeed, there are not very strict requirements on the choice of starting

material (e.g., from bi- to tetradentate monomers). On the other hand, tetragonal and tetradentate monomers are necessary to obtain 3D structures (Figure S1B).

COFs are usually synthetized as bulk materials by using boronate esters or imine bond-bridged systems as precursors (Figure 2) [62]. Yet, the so obtained COFs usually have poor electric conductivity in the *z* axis being constituted by stacked 2D layers. In this context, the introduction of imine-bridged pattern offers a feasible approach to partially extend the conjugation throughout the different layers. Indeed, whereas in boronate COFs the charge preferentially moves alongside the plane directions, imine-based COFs also allow lateral diffusion throughout the frameworks. Therefore, boronate ester-based COFs could be considered as small molecule-based electronics whereas imine-based COFs are generally described as conjugated conducting polymers [19,63].

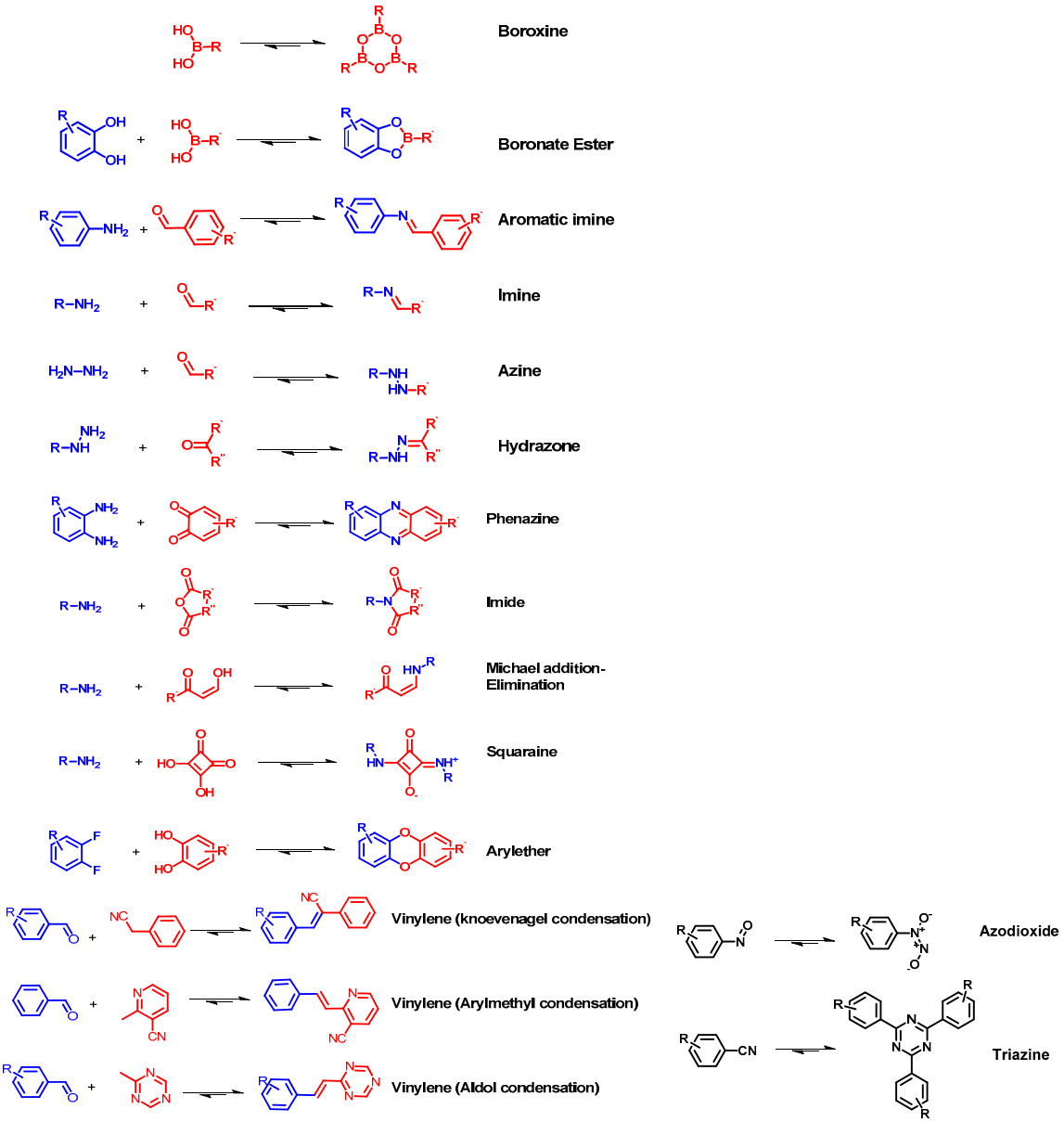


**Figure 2.** Reported linkage motifs for the realization of crystalline COFs. The reversible condensation reactions were used for the formation of a broad range of COFs.

Nanostructured systems are usually synthetized by solvothermal method allowing the latter to finely control the morphology and the crystallinity of the materials [64–66]. However, this approach includes the quite harsh experimental conditions (e.g., aggressive solvents, relatively high temperature,

using sealed vessel . . . ) as synthetic method to produce COFs Straightforwardly, researchers have been attempting to figure out new synthetic routes to obtain COFs: i.e., microwave and room temperature synthesis (which are mechanochemical and rapid solution-phase approach) and massive synthesis [67], among others [62].

Prof. Cooper and co-workers attempted first time to use microwave method by synthesizing of COF-5 and COF-102 based on boron linkage [68]. They successfully obtain COFs 200 times faster (i.e., 20 min reaction) compared to solvothermal method (72 h). Furthermore, mechanochemical synthesis is fast and environmentally friendly allowing to minimize the amount of solvents employed and the energy required throughout the synthetic procedure. COFs based on imine-bond were synthesized through this method by Biswal et al. too [69]. A simple and facile room-temperature solution-phase route for the fabrication of spherical COF-TpBD was carried out by Yan's group [70]. The obtained COFs showed quite good thermal stability and very short synthetic times (i.e., 30 min). On one hand, MW and RT synthesis could be usefully employed in the laboratory scale; on the other hand, massive synthesis method could be easily implemented for industrial production of COFs.

## 2. Dye-Sensitized Solar Cells (DSSCs)

Dye-sensitized solar cells (DSSCs) [71,72] are among the more studied photovoltaic devices among hybrid photovoltaic technologies. They were first reported by O'Regan and Grätzel in 1991 [73] and, since then, they drew a lot of attention in the scientific community: the replacement of a thin layer of titanium dioxide with a mesoporous one allowed to enhance the device efficiency up to 7.1% and the latter has reached 11% by sensitizing nanocrystalline $TiO_2$ semiconductor with Ru-based dye molecules, namely N719 or CYC-B11 [74,75]. Dye-sensitized solar cells were widely exploited due to their low-cost, relatively high solar-to-energy conversion efficiency and easy, cheap and scalable fabrication process. Up to date, the most efficient DSSC has reached 14% using porphyrin sensitizers as reported by Grätzel and co-workers [76].

With respect to the device architecture, there are five main components to constitute a classical DSSC as shown in Figure 3: a transparent conductive oxide (TCO) as substrate [77], a nanostructured *n*-type or *p*-type semiconductor as photoanode or photocatode, respectively [78,79], a visible-light absorbing dye chemisorbed onto the semiconductor surface [80], an electrolyte containing a redox mediator [81] and a counter electrode [82]. The working principle of DSSCs is inspired from natural photosynthesis. A thorough analyses of DSSC working principle falls outside the scope of the present review and it has been aplenty discussed in some excellent reviews and it is just briefly recalled hereafter [83,84]: in a working device, sunlight passes through the photoanode and causes the promotion of an electron from the fundamental state to an excited state of the dye. From the latter, the electron is injected into the conduction band of the *n*-type semiconductor (usually $TiO_2$) and, at the same time, the reduced species in the electrolyte regenerates the fundamental state of the sensitizers. From the conduction band of $TiO_2$, the electron flows through an external circuit reaching the counter-electrode where it is used to reduce the oxidized species of the redox mediator thus allowing to close the electronic circuit and produce energy [85].

### *2.1. MOFs in DSSCs*

Actually, in classical DSSCs, both MOFs and COFs, due to their chemical versatility, do not have a unique role. Indeed, they could be employed as sensitizer materials [86–89], electrolyte additives [90] or electrode materials [91–93]. In some cases, they have been employed as templates to obtain materials with tailored properties [94–97]. Hereafter, we report on the different approaches that have been exploited in literature. It is worth mentioning that, in some cases, univocal categorization is unfeasible due to the hybrid nature of the investigated material [1,98–100].

A really unique utilization of MOF was recently proposed by Sarwar et al. [101]; they employed an Al-based MOF as gelling agent in quasi solid-state DSSCs. The optimization of the MOF/electrolyte ratio allowed to modulate the photoelectrochemical response of the devices. The presence of $Al^{3+}$

cation (albeit embedded in the MOF structure) tune the $V_{OC}$ and mild the electronic recombination, reaching slightly better efficiency compared to classical DSSCs. More remarkably, a good stability was reached: just a 6% drop (after 250 h) was recorded when the devices were stressed at 60 °C.

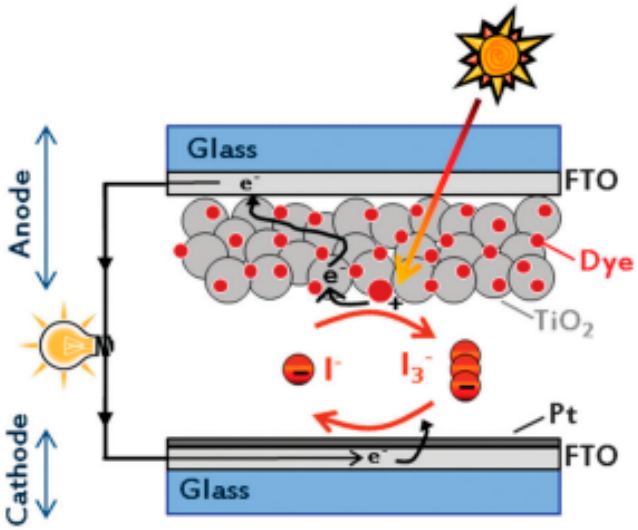


**Figure 3.** Schematic representation of the components and of the basic operating principle of a DSSC. Reproduced with permission from [71].

### 2.1.1. MOF as Photoelectrode

Titanium dioxide is the most exploited semiconducting material as photoanode in DSSCs due to its low-cost and extreme stability under solar irradiation. Additionally, being a large band-gap semiconductor (BG = 3.2 eV) [102], it does not adsorb visible light; very interestingly it could be obtained in mesoporous arrays that permit one to load very high amounts of sensitizer. $TiO_2$ is a low cost, widely available, non-toxic and biocompatible material usually employed in health care products or domestic applications [103,104]. Various alternative materials have been explored as photoanodes in DSSCs: as an example, ZnO has a similar conduction band and work function when compared to $TiO_2$ and shows the same time higher carrier mobility [105], but its low stability under solar radiation and in acidic environments as well as the likely formation of aggregates on its surface are important drawbacks [106]. Some other semiconductors have been exploited, e.g., $CeO_2$ [107], $WO_3$ [108], $SrTiO_3$ [109] and $Nb_2O_5$ [110] among others, but the photoelectrochemical performance assured by titanium oxide is still unbeaten. With respect to conventional photoelectrodic materials, MOFs have some unique features: indeed, they could simultaneously act as both electrode and sensitizers, being the metallic core directly linked to (chromophore) organic units (see also paragraph 2.1.2). The wide surface area of this class of materials could improve the dye loading as well as tune the charge transfer kinetic at the electrode/electrolyte interface.

In photocatalytic applications, semiconductor nanoparticles are generally adopted due to their large band-gap energy allowing absorption in the UV range of the electromagnetic spectrum. However, the sintering procedure required to electronically connect them to each other leads to a remarkable decrease of their surface area, then the dye-loading and light harvesting become lower. To overcome such a limitation, the use of nanostructured, porous matrices could be somehow feasible. Indeed, MOFs are suitable for this role owing to a large surface area (<1000 $m^2/g$) as well as a high porosity [111,112]. Indeed, numerous studies have been reported highlighting the promising features of MOFs as photoactive materials. For instance, Li et al. reported for the first time the application of MOFs in DSSCs [93]. They showed that a highly porous MOF known as zeolitic imidazolate framework (ZIF)-8 composed by zinc ions coordinated with four imidazolate ligands, employed as electrode/electrolyte interfacial layer, allowed for improving the dye loading and minimizing the interfacial charge

recombination due to its electrical insulating property. They synthesize an ultrathin Zn-based MOF (i.e., ZIF-8, Figure 4) that was coated onto a $TiO_2$ anode through a post-treatment approach [93].

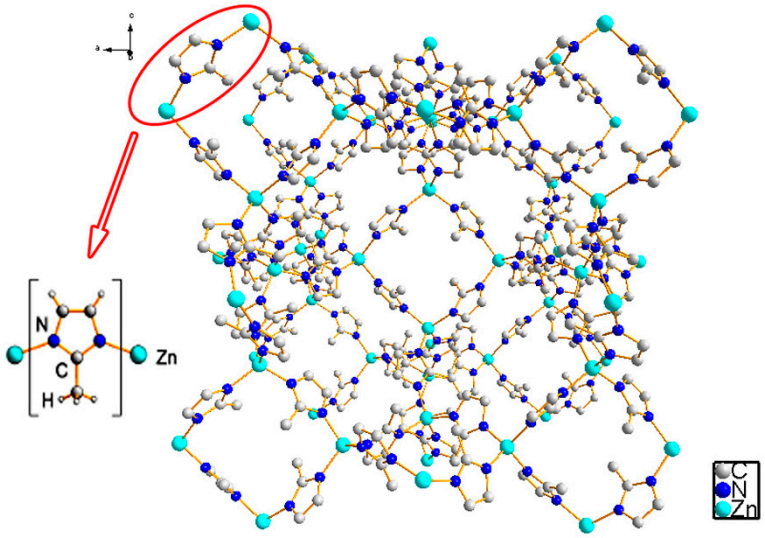


**Figure 4.** Structure of ZIF-8. Reproduced with permission from http://www.chemtube3d.com/solidstate/MOF-ZIF8.htm.

The very high specific surface area of MOFs [113–115] was proved to almost double the amount of absorbed dye (N719), i.e., from $0.71 \times 10^{-7}$ to $1.13 \times 10^{-7}$ mol $cm^{-2}$ (+43%) for the bare and modified photoanode, respectively. Unfortunately, the core/shell structure of the $TiO_2$/ZIF-8 electrode heavily hampered the injection of electrons from the sensitizer into the conduction band of $TiO_2$ by reducing the short circuit current. Very interestingly, the value of $V_{OC}$ linearly correlated with the thickness of ZIF-8 coating layer [116]. They also investigated the variation of photovoltaic performance by varying the growth time of the ZIF-8 layer. The best photovoltaic properties were achieved for a growth time of about 7 min, whereas a further increase in ZIF-8 growth time caused a decrease in both the short circuit photocurrent ($J_{SC}$) and power conversion efficiency ($\eta$) [93]. More recently, He et al. reported on the employment of UiO-66 [117] or ZIF-8 in conjunction with reduced graphene oxide (rGO) to modify the photoanode [118]. The Uio-66-RGO/$TiO_2$ and ZIF 8-RGO/$TiO_2$ were prepared by a physical mixture process to produce a slurry that was then deposited by doctor-blade onto FTO glasses. The graphene oxide-MOFs photoanode showed enhanced photovoltaic performance increasing scattering capacity of incident light as well as demonstrating low loss ratio of photo-generated electrons by small dark current and leading to a PCE close to 8%.

To further improve the morphological features of $TiO_2$, Chi and co-workers reported the use of MIL-125(Ti) along with poly(ethylene glycol) diglycidyl ether (PEGDGE) [119]. MIL-125(Ti) was used to synthesize mesoporous hierarchical $TiO_2$ (hier-$TiO_2$) photoanodes with a large surface area and a variety of nanostructures depending on the calcination procedure [120]. Simultaneously, the use of poly(ethylene glycol) diglycidyl ether (PEGDGE,) lead to the formation of larger particles and resulted in a change in the morphology of the NPs from circular plates to bipyramids. This provides better mechanical stability and faster ion transportation via Grotthus hopping compared to the ones reported by other groups [121,122]. They measured the J–V curves of the DSSCs with different photoanode structures at 1 Sun. According to the photovoltaic parameters, the hier-$TiO_2$ bilayer photoanodes boosted the solar energy conversion efficiency up to 7%, much higher than that of the nanocrystalline $TiO_2$ (nc-$TiO_2$) monolayer photoanode (4.6%). They performed durability tests for the cell efficiency, and it was observed there is no efficiency decrease at room temperature up to several days. A similar approach was attempted by Ramasubbu and co-workers [123] who prepared a 3D mesoporous $TiO_2$-Ni-MOF composite aerogels via sol–gel method and used as photoanode materials

for quasi-solid dye-sensitized solar cell (QSDSC). The photoanode was prepared by spin coated method and assembled into complete devices leading to PCE close to 9%, higher than the one obtained with unmodified aerogels (7%), ascribable to increased photocurrent density, reduced charge-transfer resistance and suppressed electron recombination as proved through photocurrent density–applied voltage curves and electrochemical impedance measurements. In Table 1, the most effective MOFs implemented as photoelectrodes in DSSCs are summarized.

**Table 1.** List of MOFs effectively employed as photoelectrodes in DSSC. For sake of brevity, the SBUs of the MOF (i.e., metal and the organic linker) are indicated separately. Note that the reported values of photoconversion efficiency cannot be compared to each other, even though they could shine light on the potentiality of this class of material.

| Special Role | MOFs | | η (%) | Ref. |
|---|---|---|---|---|
| | Metals | Organic Linkers | | |
| ***Interfacial Layer*** | Zn | ZIF-8 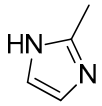 | 5.34 | [93] |
| | Zn | 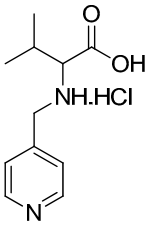 | 2.34 | [124] |
| ***Scattering Layer*** | Zn | MOF-5 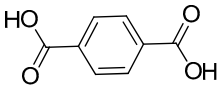 | 3.67 | [125] |
| | Ti | MIL-125(Ti) 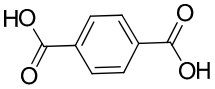 | 7.1 | [126] |
| | Zn | 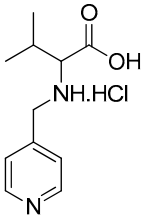 | 0.15 | [92] |
| | Cu | 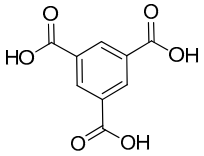 | 0.008 | [86] |
| | Cu | 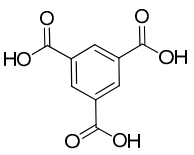 | 0.27 | [126] |

**Table 1.** *Cont.*

| Special Role | MOFs | | η (%) | Ref. |
|---|---|---|---|---|
| | Metals | Organic Linkers | | |
| | Cu | 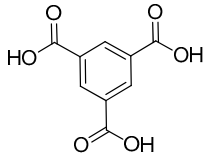 | 1.22 | [88] |
| | Ru | 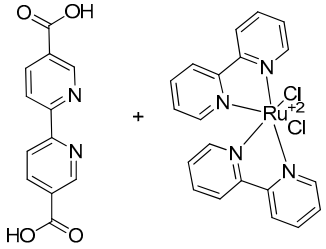 | 0.125 | [87] |
| | Zn | 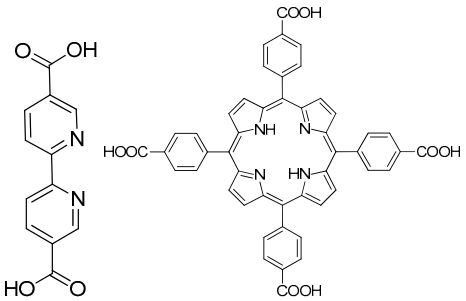 | 0.86 | [127] |
| | Cu | 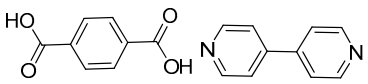 | 0.1 | [128] |

### 2.1.2. MOFs as Sensitizers

In dye-sensitized solar cells, the sensitizer plays a crucial role and its choice is not trivial. In fact, a good dye should fulfil some very strict requirements [129–132]. First of all, it should possess a very high molar extinction coefficient and a broad absorption in the visible/near infrared (NIR) region of the solar spectrum in order to catch as much radiation as possible. It should also possess one or more anchoring units in order to be firmly bound to the semiconductor surface and to assure a proper matching between the HOMO or LUMO level of the sensitizer with the valence or conduction band of the semiconductor. At this regard, a sensitizer should be properly designed in order to be able, on the one hand, to assure fast and quantitative charge injection into the semiconductor and, on the other hand, to be easily regenerated by the redox mediator [133,134]. Furthermore, a dye should be thermally, photochemically and physically stable once chemisorbed onto the semiconductor surface and it should help to enhance the electrode wettability with respect to the electrolytic solution. Both metal-organic and fully organic sensitizers have been deeply investigated and their properties tuned; yet, they somehow suffer for both thermal and photophysical stability. In this context, MOFs offer a viable alternative due their extremely robustness; additionally, their high ordering (both on medium and long range) could create channels that the electrolyte could soak assuring a very fast regeneration of the excited state of the sensitizer.

Ruthenium-based sensitizers assure a very high photoconversion efficiency, but they partially limit the long-term stability of the device due to the desorption from photoanode surface when in contact with an organic-based electrolyte, i.e., ACN or MPN. Additionally, ruthenium is a quite rare

metal and its cost could prevent a large-scale production of DSSCs. Nowadays, organo-metallic sensitizers have been replaced by metal-free dyes keeping relatively high efficiency. These molecules are generally constituted by an electron donor group (e.g., triphenylamine) linked to an acceptor group (e.g., cyanoacrylic acid) [135–137] generating an acceptor-π-donor system (A-π-D) with the acceptor moiety close to the electrode surface to assure an effective charge injection. In this respect, MOFs could be used as a sensitizer by using different dye molecules as a building blocks extending the spectral response of the $TiO_2$ to the visible region.

The light harvesting capacity of MOFs is basically based on the electronical and morphological features of the organic linker. The most common ones are capable of absorbing light only from UV to blue regions. Recently, some novel structures e.g., 2,5-dihydroxyterephthalic acid ($H_4$DOBDC) and 2-aminoterephthalic acid ($NH_2$-bdc) were synthetized to further extend the absorption over the whole solar spectrum [98,99]. In 2014, Gao et al. reported on the synthesis of an organic linker (i.e., $H_4$DOBDC) to build up a *p*-type MOF (i.e., Ti(IV)-based NTU-9) with visible-light photoresponse capabilities: the latter showed a strong absorption in the visible region (up to 750 nm). To further exploit the absorption spectra Long and co-workers synthesized a MOF in which $Zr_6O_{32}$ units were linked each other with $NH_2$-bdc (or 2-aminoterephthalate): UV-vis diffuse reflectance studies revealed that this MOF has an optical bandgap of 2.75 eV (absorption peak centered at 450 nm) [100].

In 2012, Kundu et al. reported, for the first time, on the implementation of a ZnO-based photoanode using MOFs that was not sensitized with any dyes (Figure 5) [92]. Indeed, MOFs behaved as a real sensitizer. They obtained hexagonal column shaped, rod-shaped or elliptical structures of ZnO as a result of different synthetic environment (i.e., under nitrogen or air) and starting material ($ZnCl_2$ or $ZnBr_2$). The so-obtain photoanodes were able to effectively absorb visible light between 510 and 605 nm. Nevertheless, the photoconversion efficiency remained very low due to a poor charge transport features of the hybrid electrode. Lee et al. tried to overcome such an issue by an unconventional but very promising approach: they produced a $TiO_2$-based DSSC in which a thin layer of copper-based MOF (i.e., copper(II) benzene-1,3,5-tricarboxylate) behaved as a light-absorber [86]. The MOF film was deposited by a layer-by-layer method and further doped with iodine to enhance its conductivity and control charge transfer reactions. I-doped device allow to obtain an overall photoconversion efficiency up to 0.26% ($J_{SC}$ = 1.25 mA·cm$^{-2}$, under 1 Sun illumination) that consist in a 40-fold increase compared to the undoped DSSC. This was ascribed to a reduction of the charge transfer resistance as proved by electrochemical impedance spectroscopy (EIS).

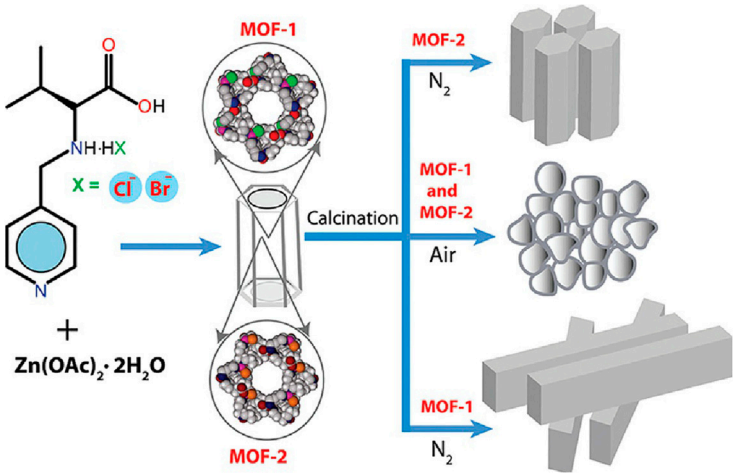


**Figure 5.** Synthetic routes to different ZnO nanostructures through one-step thermolysis of porous homochiral MOFs under $N_2$ or air. Reproduced with permission from [92].

Lee et al. reported on a $TiO_2$-MWCNTs composite photoanode sensitized with a Cu-based MOF (i.e., copper (II) benzene-1,3,5-tricarboxylate) [126]. Since Cu-MOFs have an insulating behavior [86],

iodine doping was required to enhance the conductivity of the obtained film. Even if the bare $TiO_2$-MWCNT composite film did not show any significant light absorption, after sensitization with Cu-MOFs, the composite film presented visible light absorption at around 680 nm [93]. Yet, the so obtained device based on $TiO_2$/MOF composite a quite low photoconversion efficiency (nearly 0.3%) that was then boosted up to 0.46% by using a MWCNT nanotubes composited anode. In successive study, the same authors used Ru instead of Cu as metal linker. Both HOMO and LUMO energy levels of the Ru-based MOFs were found to be more appropriate with respect to $TiO_2$ conduction band (Figure 6). The latter evidence led to a power conversion efficiency up to 1.22% which is three times higher than the previous Cu-MOF-based device [88]. In a different study, Maza and co-workers employed a Ru-based MOF (namely, Ru(II)$L_2L'$ (L = 2,2′-bipyridyl, L′ = 2,2′-bipyridine-5,5′-dicarboxylic acid) as sensitizer on a $TiO_2$ electrode [87].

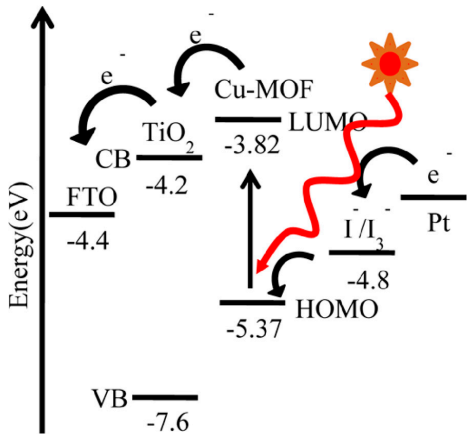


**Figure 6.** Energy diagram of $TiO_2$−MOF system showing the suitable energy cascade for unidirectional flow of charge carriers. Reproduced with permission from [126].

Porphyrin-based MOFs can produce quite limited photocurrents under visible light (PCE: 0.0026–0.45%) as reported by Wöll [89,138], Allendorf [139] and others [140]. On the other hand, $Ru(bpy)_3^{2+}$-based MOFs have slightly better PCE [87]. Their relatively low photoelectrochemical performances could be ascribed to the slow exciton migration and ineffective charge transport properties of 3D porous frameworks [89,138]. Recently, Gordillo et. al. reported on a spontaneous solvothermal growth of (100) oriented PPF-11 [50] films onto a ZnO/FTO electrodes [127]. The so obtained MOF-sensitized photoanodes displayed unpredictable phototoelectrochemical parameters (i.e., $J_{SC}$ = 4.6 mA·cm$^{-2}$; $V_{OC}$ = 476 mV; PCE = 0.86%). These values are 1000 and 300 times greater than conventional devices concerning current density and efficiency, respectively. Some further experiments are still required to clarify such results; the authors claimed better charge separation and faster charge transport/injection features assured by the highly oriented MOF structure.

As known, MOFs could be employed as precursors in the synthesis of MOF/$TiO_2$ composites behaving as both anode and sensitizer [92,125,141,142]. Khajavian and Ghani reported on the application of a polycrystalline and highly oriented copper-based MOF [i.e., $Cu_2(bdc)_2(bpy)]_n$ thin films onto mesoporous titania surface [128]. The MOF was synthesized by a layer-by-layer approach and it is possible to regulate shape evolution of MOF crystals within the films using acetic acid and pyridine as capping agents added to metal solution. Indeed, the former could drive the growth and the orientation of MOF crystal whereas the latter allows to obtain leaf-structured crystals. Even if this approach is very interesting thanks to its cheapness and scalability, the implementation of MOF/$TiO_2$ composite in a DSSC led to very poor photoconversion efficiency (lower than 0.1%) mainly because of the thinness of deposited layer (lower than 100 nm), giving insufficient light absorption, and the not-optimized MOF/$TiO_2$ interface. Nevertheless, a further engineering of the deposition method could lead to improved photoconversion features.

As already evidenced in the previous section, metal-organic frameworks are complex molecules with highly tunable properties. This tunability could be largely exploited in order to design molecules with tailored features. In this context, Du et al. investigated the effect of different ions, i.e., K(I) and In(III), during the growth process of a single crystal heterometal-organic framework as sensitizer in DSSCs [143]. The two MOF were named $[In_{0.5}K(3\text{-qlc})Cl_{1.5}(H_2O)_{0.5}]_{2n}$ and $[InK(ox)_2\text{-}(H_2O)_4]_n$ (with 3-Hqlc = quinoline-3-carboxylic acid; $H_2ox$ = oxalic acid). The so-obtained MOFs were then implemented in a (co)sensitized DSSC (along with a classical dye like N719) in order to extend the absorption region within the ultraviolet and blue-violet region of the solar cells. Indeed, the energetic matching between the energy states of MOF and $TiO_2$ allows to extend the photoelectrochemical response of the device below 350 nm. By means of that, a photoconversion efficiency higher than 8% was achieved. Additionally, the investigated MOFs exhibit tunable luminescence (from blue to yellow to white) as a function of temperature. These very interesting features could open the doors to the application of MOF in different fields, e.g., light emitting electrochemical cells/diodes, LEEC [144] or LED [145], respectively [146].

Even if MOFs have been proved to be effective photosensitizer material, the specific role and potential effect of unreacted MOF precursor (considering the in-situ growth of the material) on both device performance and stability has not been explicated so far. In order to clarify this point, Spoerke and co-workers isolated MOF crystals to be anchored as a photosensitizer onto the photoanode surface [139]. More in details, they synthesized the pillared porphyrin framework (PPF) MOF (Zn-based) through solvothermal method (heated in a closed vessel at 80 °C for 72 h) from a solution of Zinc(II) meso-tetrakis(4-carboxyphenyl)porphyrin (Zn-TCPP), $Zn(NO_3)_2{\cdot}4H_2O$, and 4,4′-bipyridine in di-ethyl-formamide (DEF) and ethanol. To rule out the effect of the eventual presence of unreacted precursor in the sensitization solution, they prepared MOF crystals with and without a known excess of linker. The obtained MOFs were implemented as sole sensitizer in complete $TiO_2$-based DSSC and efficiency was obtained as a 0.0023 (±0.0003) with PPF-MOF-sensitized solar cell, 0.0011 ± 0.0002 for unsensitized $TiO_2$.

It is worth mentioning that, up to now, MOFs (in the sensitizer role) have been mainly employed in liquid-junction DSSC. Ahn et. al. reported on, for the first time, MOF-sensitized based solid-state photovoltaic cell [147]. More in details, conductive cobalt-based MOFs (Co-DAPV) consisting of Co (II) ions and a redox active di(3-diaminopropyl)-viologen (i.e., DAPV) ligand were investigated. This MOF was proved to effectively match the energetic level of $TiO_2$ leading to a power conversion efficiency of the solid junction solar cell was measured up to 2% which is higher than the homologous liquid-junction counterparts, opening the doors to further investigation on this topic (Figure 7).

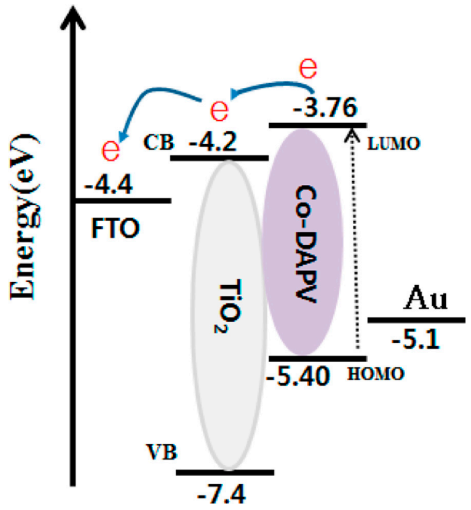


**Figure 7.** Energy level diagram showing the band edge alignment at TiO2-DAPV heterojunction, showing favorable energy cascade for unidirectional charge transfer. Reproduced with permission from [147].

In a classical DSSCs, the role of the sensitizer is played by an organic or metallorganic molecular dye. Yet, a different approach has been recently exploited consisting in the employment of inorganic quantum dots (QDs) as effective sensitizer in DSSCs [12,148]. Indeed, QDs offered various advantages such as multiple exciton creation, surface effect, quantum size effect, and tunnelling effect that could be hardly reached by using a molecular dye [148–150]. Additionally, they are much more stable considering their intrinsic inorganic nature. Nevertheless, once implemented in complete device (i.e., QD-sensitized solar cells, QDSSCs) this material assured lower photoconversion efficiency because they possess relatively low molar extinction coefficient and a quite sharp absorption spectrum; furthermore, the presence of surface states that behaves as trap states partially prevent an effective charge injection [150] and they could be hardly anchored onto mesoporous $TiO_2$ leading to an inhomogeneous covering of the electrode surface [151]. In this context, MOFs could be advantageously employed to improve the light harvesting efficiency as a consequence of the energy transfer from QDs to MOFs. Jin, and co-workers reported on the synthesis of a porphyrin-based MOF functionalized with CdSe/ZnS core/shell quantum dots (QDs) and its implementation in complete device [152]. The broad absorption band of the QDs in the visible region suggested excellent coverage of the solar spectrum via QD−MOF hybrid structures. Indeed, QD-MOF hybrids allowed to harvest photons even at wavelengths in which the MOF has a low or no absorption. They were able to obtain very high quantum efficiencies (up to 84%) by altering size of the QDs. Quite recently, Kaur et al. employed an europium-based MOF as a co-sensitizer in quantum dot DSSC (QD-DSSCs) [153]. In details, Eu-MOF acted as a supporting layer for CdTe QDs. Remarkably, the implementation of CdTe@Eu-MOF sensitizer in complete device led to a significant decrease in charge recombination allowing to obtain an 80% photoconversion efficiency compared to device not embodying Eu-MOF (i.e., 3.0% vs. 1.7%, respectively). The same authors replaced the Eu-based MOF with a Ti-based one (namely NTU-9) that allowed to obtain a more broadened absorption spectra leading to quite good results [154]. Even if they recorded very high photocurrent density (up to 23 $mA{\cdot}cm^{-2}$), the devices suffer for very low FF, lower than 30%. Therefore, before further exploiting these materials as sensitizers in QD-DSSCs, an optimization of the anode/sensitizer/electrolyte interface is required. In Table 2, the most effective MOFs implemented as sensitizers in DSSCs are summarized.

Metal-organic frameworks could also be employed to synthesize composite material as photoanodes for DSSCs. In a recent study, sol–gel synthesis of $TiO_2$ aerogel–MOF (i.e., a Zn-based MOF, namely Zn(N-(4-pyridylmethyl)-L-valine·HCl)(Cl)]$(H_2O)_2$) nanocomposite have been used as photoanodic materials in quasi-solid dye-sensitized solar cells (QSDSSC) [124]. Thanks to their high surface area, MOF could be effectively employed to load dye molecules. Even if the dye-loading is higher compared to $TiO_2$ electrode. once implemented in a QSDSSC, the MOF-modified electrode showed a photoconversion efficiency up to 2.34% that is lower compared to classical photoanode (i.e., 3.0%) because of a quite inefficient collection charge efficiency; indeed, the presence of MOF leads to slower photoinjected charge diffusion throughout the photoanode because Zn anions could behave as trap states. A new approach, proposed by Li and co-workers [125], consists in using MOFs as a scattering layer in ZnO-based DSSCs. Hierarchical ZnO parallelepipeds were produced using MOF-5 precursor. It was noted that the implementation of such a scattering layer improved the cell efficiency from 3.15% to a 3.67%.

**Table 2.** MOFs effectively employed as sensitizers in DSSC. For sake of brevity, we prefer to report the metal and the organic linker separately. The reported values of photoconversion efficiency could not be compared between each-others, yet they could shine light on the potentiality of this class of material.

| MOFs | | η (%) | Ref. |
|---|---|---|---|
| **Metals** | **Organic Linker(s)** | | |
| **In/K** | 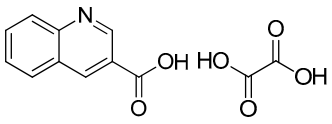 | 8.07 | [143] |
| **Zn** | 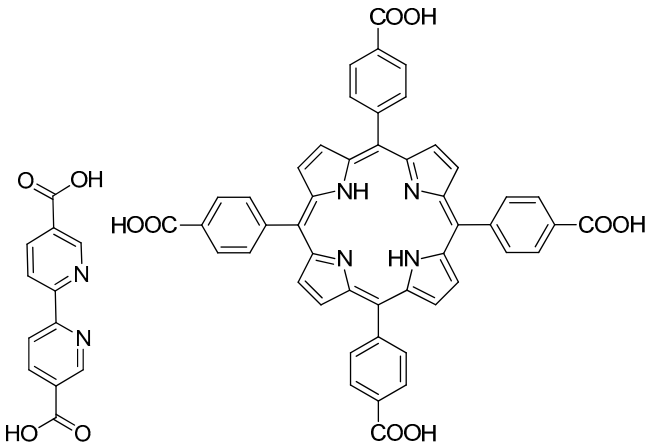 | 0.0023 | [139] |
| **Co** | Co-DAPV MOF 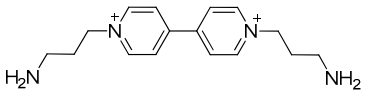 | 2.1 | [147] |
| **Eu** | Eu-MOF 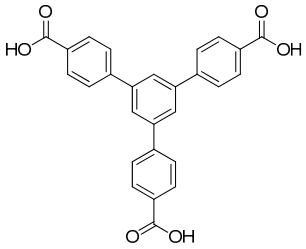 | 2.2 | [153] |
| **Ti** | titanium-based MOF 'NTU-9,' 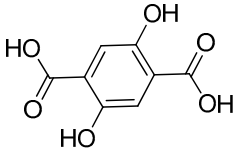 | 3.20 | [154] |
| **Zn** | 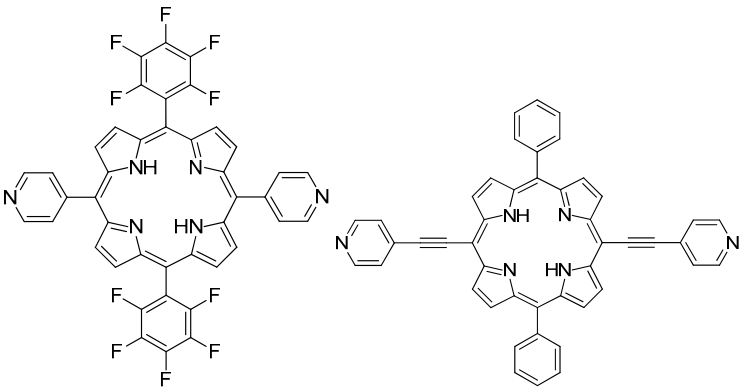 | n.a. | [152] |

### 2.1.3. Counter-Electrode CE

Besides photoanode and sensitizers, the counterelectrode (CE) plays a crucial role in a DSSC because it should quantitively regenerate the redox mediator avoiding any current loss at the CE/electrolyte interface. To behave properly, a CE should assure a wide surface area, a good contact with the electrolytic solution and a fast kinetic of the charge transfer reactions. To perform this role, scientists mainly focused their attention on platinum. Indeed, platinum, in the form of thin layer, is an extraordinary catalytic compound in DSSCs [155,156] to regenerate the redox mediator at the CE. On the other hand, Pt is a noble metal, very rare on Earth and relatively expensive (considering large-scale production). Therefore, in order to reduce the costs of CEs, some studies reported on the synthesis and the implementation of Pt-free counter-electrodes. These include graphene [157], carbon nanotubes [158], metallic PEDOT [159] and transition metal sulphides [160]. The more promising class of alternative materials is represented by metal sulphides, due to its low production cost, great availability, high stability and durability [160–162].

In this context, cobalt sulphide (CoS) is one of the most exploited materials both in *n* [160] and *p*-DSSCs [163]. For example, Grätzel electrochemically deposited CoS counter-electrodes obtaining a photoconversion efficiency up to 6.5%. Starting from this, Hui Hsu and co-workers obtained the highest power conversion efficiency ever reported for CoS-CEs (i.e., nearly 8.1%) by preparing CoS nanoparticles via a surfactant-assisted synthesis in which ZIF-67 (a cobalt-based MOF, namely $Co(mim)_2$, mim = 2-methylimidolate) was used as template. The relatively high efficiency is consistent with an increase in both $V_{OC}$ and FF values. This proved that the reported synthetic method could be considered as a promising approach [164]. ZIF-67 is a common type of MOF constituted by cobalt metal linked with four nitrogen atoms (Co-N4) to tetrahedral frameworks [165]. A similar approach was employed by Liu and co-workers to obtain $MoS_2@Co_3S_4$ composites employing ZIF-67 as both template and cobalt source [95]. The composites showed promising synergistic effect on the catalysis of triiodide reduction. Dye-sensitized solar cells fabricated with $MoS_2@Co_3S_4$ reached a PCE of 7.86%, slightly higher than the Pt-based counterpart. This composite material is a promising candidate as an efficient and low-cost counter electrode material.

Selenization or sulfurization process of ZIF-67 could be a feasible approach to produce Co-based selenide (sulphide)/N-doped carbonaceous hybrid material. Wang and co-workers synthesized $CoSe_2$/NC and $CoS_2$/NC (NC; N-doped carbon) electrocatalytic film as counter-electrode in DSSCs [166]. These composites were proved to assure huge catalytic activity and high conductivity and a PCE of 9% was achieved. Interestingly, $CoSe_2$/NC were more effective than both Pt-based and $CoS_2$/NC-based CEs (8% and 8.7%, respectively). It is worth mentioning that this work opens the doors to the use of selenium-based materials in place of the more exploited sulphur-based counterparts (Figure 8). More recently, Wu et al. reported $CoSe_2$-D as effective MOF-derived CEs [96]. They synthesized the MOF precursor directly on FTO glass via electrodeposition followed by a solvothermal process and then in-situ selenized. The so-obtained film is characterized by a porous structure leading to an easier diffusion of iodine-based redox couple and, straightforwardly, to very promising PCE (close to 7%).

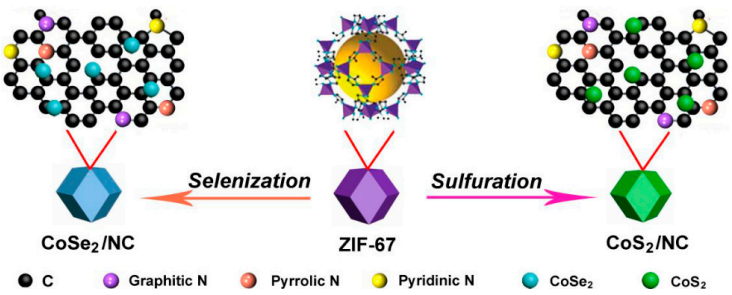


**Figure 8.** Illustration of synthesis and structure for preparing CoSe2/NC and CoS2/NC. Reproduced with permission from [166].

It is worth mentioning that MOFs could also be very useful during the preparation step if not directly embodied in a cell component. A new class of MOF is the so-called surface-anchored metal-organic framework thin film (SURMOF). They have received substantial attentions in electrical application, and they showed enhanced catalytic activity and higher electrical conductivity compared to classical MOFs when employed as CEs in DSSCs. Very recently, Ou et al. present a facile method to prepare CoS@N-doped carbon-based counterelectrode starting from a cobalt-based MOF (namely. PIZA-1) [167]. Briefly, the partial sulfurization of the MOF lead to a transparent thin film that acted as cathodic material in a conventional DSSC (Figure 9). They observed that CoS@N-doped carbon film assured extremely good catalytic performances toward the reduction of triiodide as a result of a synergetic activity of homogeneous CoS nanoparticles, strong adhesion onto glass substrate and low resistance at the interface with FTO layer. These features result in a photoconversion efficiency of 9.11% (compared to 8.04% with convention Pt-based CEs). Tian et al. also presented Pt-doped metal−porphyrin framework thin films for efficient bifacial dye-sensitized solar cells [168]. The transparent 2D MOF Zn-TCPP thin film was obtained on FTO glass using the van der Waals liquid-phase epitaxial growth approach. The obtained highly Pt-dispersed Zn-TCPP (Zn-TCPP-Pt) thin film for CE in DSSCs showed similar catalytic activity compared to conventional Pt-based CEs but a better light transmission capacity. Power conversion efficiencies of the Zn-TCPP-Pt thin film CE was measured 5.48 and 4.88% under front-side and rear-side irradiation, respectively. To overcome the poor conductivity and short chemical stability of $CoS_2$, Cui et al. [169] exploited a groundbreaking approach: they loaded $CoS_2$ into carbon nanocages using ZIF-67 as surfactant. They tested different treatment times and after 4 h they obtained the highest photovoltaic conversion efficiency (PCE) of 8.20%, higher than those of DSSCs made up of other CoS2 CEs and Pt-based DSSC (7.88%). Zhong and co-workers applied the same concept to quantum dot DSSCs (QD-DSSCs [170]: indeed, they grew crystalline ZIF-67 framework by using layered double hydroxides (LDHs) as scaffold and Co, N co-doped porous carbon materials as active material. The latter showed a very good electrocatalytic activity in the reduction of plysulphide-based electrolyte leading to a PCE higher than 13.5% ($J_{SC}$ = 25.93 mA/cm$^2$, $V_{OC}$ = 0.778 V, FF = 0.672).

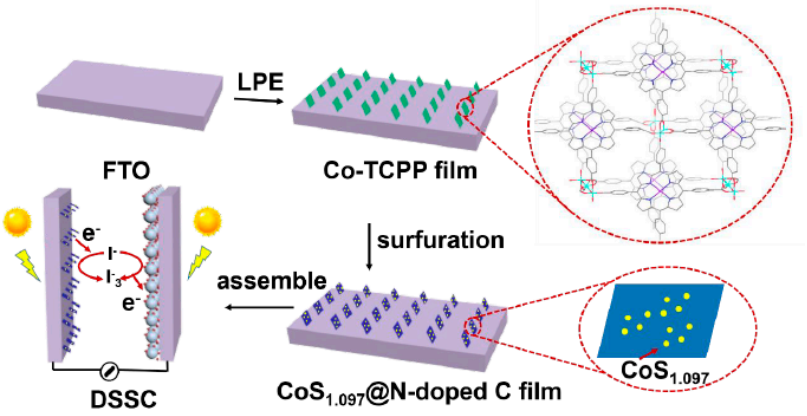


**Figure 9.** Schematic illustration of preparation process of CoS1.097@N-doped carbon film CE for DSSCs. Reproduced with permission from [167].

By employing a similar approach, Li and co-workers reported on the employment of MOF-derived Co,N-bidoped carbons as effective CEs in quantum dot DSSCs (QD-DSSCs) [171]. A bimetallic (i.e., Zn and Co) zeolite-type MOF were pyrolyzed to obtain the desired doped material showing a homogeneous di dispersion of the doping atom in the carbon matrix. Additionally, this method assured to obtain large surface area and good electronic properties leading to an overall photoconversion efficiency up to 9% (i.e., 9.12%, $V_{OC}$ = 0.635 V, $J_{SC}$ = 26.2 mA·cm$^{-2}$, FF = 0.55). ZIF-8 assured high photocatalytic performance due to its microporous structure a surface and wide surface area. Yet, micropores could lead to substantial limitation in mass transfer, especially when bulky redox

mediators (e.g., Co or Cu complexes) are employed. To overcome such a problem, Kang et al. modulated the dwelling time of Zn in ZIF-8 [172]. The longer dwelling time lead to the formation of a mesoporous structure without sensibly influence the active area. Photoconversion efficiency up to 9% was reached when these CEs were implemented in complete device with a $I^-/I_3^-$ redox mediator. This evidence proves that also the photocatalytic activity toward triiodide was improved going from micro to mesoporous electrodes.

It is worth mentioning that a serious issue to be solved to enhance the photoconversion efficiency of QDSSCs concerns the development of an electrocatalysts with more active sites, high conductivity and good photoelectrochemical and thermal stability. Very recently, Wang et al. reported on the implementation of copper NPs@carbon nanorod (Cu@CNR) composites synthetized by direct pyrolysis of HKUST-1 (copper-based MOF) [173]. Cu@CNR showed high catalytic activity towards polysulfide reduction. This approach allows to obtain a large amount of $Cu_xS$ active sites whose charge transfer ability is enhanced by the presence of CNRs as supporting material leading to an overall photoconversion efficiency close to 10%. In Table 3, the most effective MOFs implemented as counter-electrodes in DSSCs are summarized.

**Table 3.** MOFs effectively employed as counter-electrodes in DSSC. For sake of brevity, we prefer to report the metal and the organic linker separately. The reported values of photoconversion efficiency could not be compared between each-others, yet they could shine light on the potentiality of this class of material.

| MOFs | | η (%) | Ref. |
|---|---|---|---|
| **Metals** | **Organic Linkers** | | |
| **Co** | PISA-1 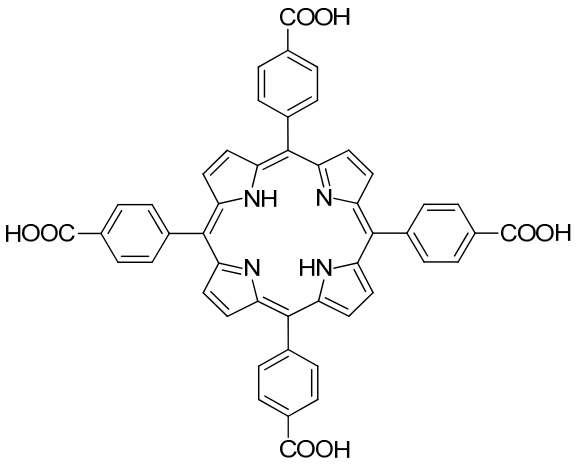 | 9.11 | [167] |
| **Co** | ZIF-67, 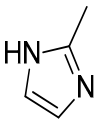 | 8.2 | [169] |
| **Co**<br>**Zn** | ZIF-67, ZIF-8 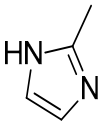 | 13.50<br>9.12 | [170]<br>[171] |
| **Zn** | Carbonaceous-ZIF-8 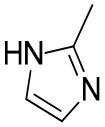 | 9.03 | [172] |
| **Cu** | HKUST-1 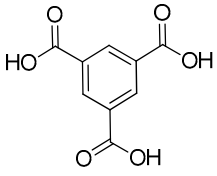 | 9.50 | [173] |
| **Co** | ZIF-67 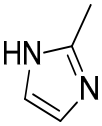 | 7.58 | [174] |

**Table 3.** *Cont.*

| MOFs | | η (%) | Ref. |
|---|---|---|---|
| **Metals** | **Organic Linkers** | | |
| **Zr** | MOF-525 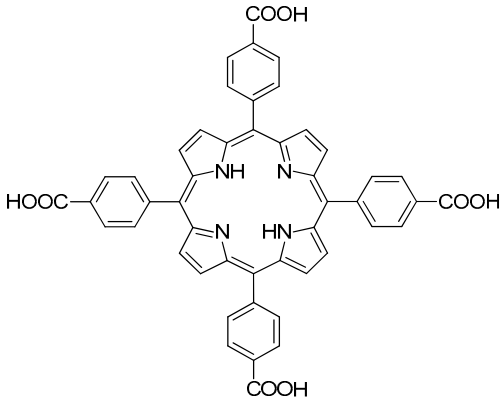 | 9.75 | [175] |
| **Zn** | | 5.48 | [168] |
| **Ni/Co** | $NiCo_{0.2}$/MOF 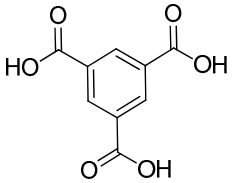 | 9.30 | [176] |

Usually, MOFs-derived materials are obtained by direct carbonization/sulfurization methods; indeed, the so-synthetized nanoparticles tend to agglomerate and collapse. This might cause the decrease of the effective surface area and the growth of a physical barrier for the electrolyte diffusion [177]. Porous 1D nanomaterials are known as one of the most promising electrocatalytic materials in energy-related applications [178,179]. Unfortunately, synthesis of 1D structure materials starting from individual MOFs is very challenging due to fast nucleation and growth assured by the presence of the MOF typical porous structure. Straightforwardly, scientists' attention was focused on 2D structures, such as nanotubes (NTs). Very recently, metal selenides have been employed as CE materials in place of the more exploited sulphides. Li et. al. optimized a facile synthetic approach to obtain hierarchical hollow CoSe nanoparticles embodied into nitrogen-doped porous carbon anchored onto nitrogen-doped carbon nanotubes (CoSe@NPC/NCNTs) as CE material in DSSCs [180]. They used a cobalt-containing MOF, i.e., ZIF-67, and polypyrrole (PPy) as template and nitrogen source, respectively, to obtain the ZIF nanocrystals growing along the surfaces of PPy to constitute core-shell nanotubes. The tubular structure and the wide surface area of these material boosted the electron transfer and improved charge mobility throughout the NT leading to good photoconversion efficiency (h = 7.6% compared to 7.3% with Pt-based CEs).

It is worth mentioning that MOFs could be directly used as counter-electrode in place of Pt because they could somehow play the role of electrocatalyst toward the reduction of triiodide. In a pivotal work, Chen et al. reported on the synthesis of a carbon cloth/MOF (i.e., sulfonated poly(thiophene-3-[2-(2-methoxyethoxy)ethoxy]-2,5-diyl) (s-PT), MOF-525/s-PT) composite film deposited on a flexible substrate [175]. They proved that, on the one hand, carbon fibres in CE supported electron transfer behaving as a conductive core, whereas, on the other hand, MOF-525/s-PT acts as the effective catalyst for the reduction of $I_3^-$. The investigated MOF-525/s-PT composite counter electrode allowed to obtain an amazing cell efficiency, as high as 9.75% that is higher than traditional Pt-based CE (8.21%). Very interestingly, Liu and co-workers employed bimetallic (i.e., nickel and cobalt) MOFs as counter-electrode (Figure 10) [176]. More in details,

they optimized the Co/Ni ratio into the framework and obtained a photoconversion efficiency up to 9.3% when a $NiCo_{0.2}$-based MOF supported onto carbon behaves as CEs showing an extremely good photoelectrochemical stability in contact with $I_3^-/I^-$ electrolyte. The latter value is 16% higher if compared to the one obtained with conventional Pt-CEs. The above-mentioned results should be considered just as a starting point, yet they proved that MOF (or at least MOF supported on carbonaceous or plastic material) could be seriously investigated as an effective low-cost and feasible alternative to platinum as counter-electrodes in DSSC.

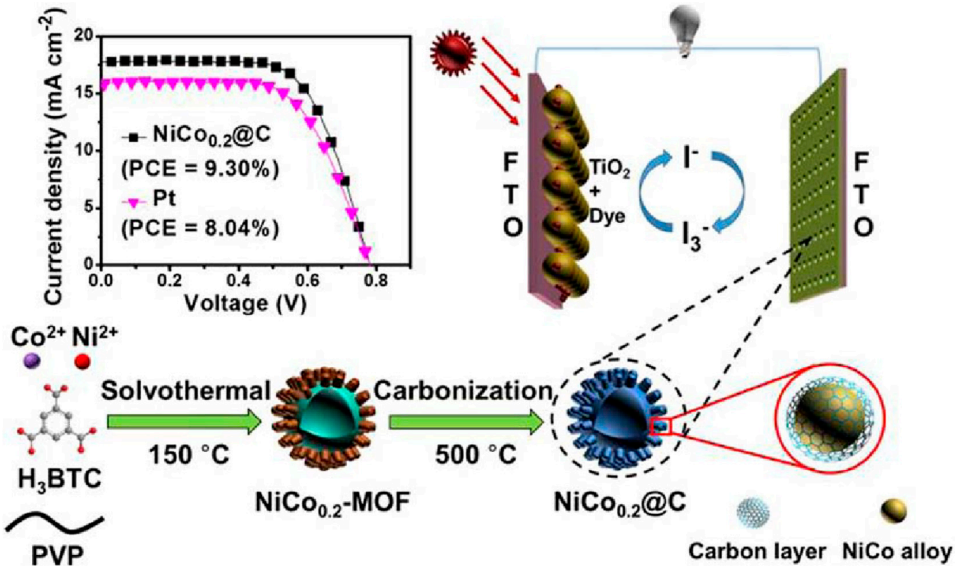


**Figure 10.** Schematic illustration of the formation process of $NiCo_{0.2}$@C and cell performance. Reproduced with permission from ref. [176].

### *2.2. Covalent Organic Frameworks (COFs) in DSSCs*

Differently from MOFs, just few examples have been reported concerning the implementation of covalent organic frameworks in photovoltaic devices. Most of the published studies concern the investigation of their photoelectrochemical properties, nevertheless, we decide to tackle the latter being an interesting starting point for further optimization.

#### COFs as Photoactive Materials

Jiang et al. reported, for the first time, the synthesis of a photoconductive COF (i.e., PPy-based COF) obtained by self-condensation of pyrene diboronic acid to constitute a boroxine-linked COF [180]. This was obtained as micrometric cubic crystals. They measured the photoconductivity of PPy-COF by evaporating a thin film onto an Al electrode and then covered the COF with an Au layer. If irradiated with a xenon lamp (in the visible region) the COF-modified Al-electrode showed a linear I-V response. Additionally, the on-off ratio was not modified even after multiple switching procedures. As already evidenced in the MOF section, the most appealing feature to further develop covalent organic frameworks in DSSCs is the higher stability assured with respect to conventional dyes as well as the opportunity to tune both their photo- and electrochemical properties.

Another photoactive COF was presented by Ding and co-workers: they synthesized COF using Ni-phthalocyanine through condensation reaction with 1,4-benzenediboronic acid (BDBA) [181]. This COF, implemented in an electrode, exhibits a photocurrent of 3 μA when irradiated with a xenon lamp. In a subsequent study, the same authors discovered that pthalocyanine-based n-channel 2D-NiPc-BTDA COFs allowed a faster transport of electrons due to the AA-type stacking. Additionally, the latter absorbs light over a wide range of wavelengths up to 1000 nm [182]. In place of phthalocyanine COFs, porphyrin-based ones were made by condensation reaction with benzene diboronic acid (DBA)

to obtain photoactive COFs with different electron and hole mobility following on from the nature of the metal in the porphryin building block [183].

There are various examples of conductive and photoactive COFs. Nevertheless, their assemblage into complete devices is very challenging due to their insolubility being hardly coated (homogeneously) onto the surface of electrodes or conductive substrates. Following on from this evidence, a feasible approach to avoid the above-mentioned issues, is to directly grow the COF onto the electrode surface. Indeed, Dichtel and co-workers were able to grow oriented COF thin films by using 1,4-phenylenebis(boronic acid) (PBBA) with 2,3,6,7,10,11-hexahydroxytriphenylene (HHTP) (to produce COF-5) and Ni-phthalocyanine-PBBA COF by incorporating single-layer graphene (SLG) supported on copper, silicon carbide, and silicium dioxide substrates under operationally simple solvothermal conditions [184]. Remarkably, COF layers deposited onto SLG showed improved crystallinity if compared to COF powders. The Ni-phthalocyanine-PBBA-based COF on SLG/$SiO_2$ films absorbed strongly over the visible range of the spectrum. Therefore, porous phthalocyanine COFs are depicted as suitable candidates to be implemented in organic photovoltaics.

Jiang and co-workers synthetized fullerene-loaded CS-COF, a conductive and chemically stable COF obtained by the co-condensation of triphenylene hexamine (TPHA) and *tert*-butylpyrene tetraone (PT) [185]. Experimentally, the dispersion of CS-COF*C60 in N-methyl-2-pyrrolidone was performed by stirring the solution at 80° C under argon flux for 1 week. Then, a mixture of PCBM in *o*-dichlorobenzene (40 mg·$mL^{-1}$) and the obtained suspension (40 mg·$mL^{-1}$ for CS-COF·C60) were spin coated (1000 rpm, 30 s) onto an ITO substrate for organic solar cells. They built up a 1 $cm^2$ sandwiched device with a Al/poly(methyl methacrylate (PMMA) as a glue called CSCOF*C60/Au cell geometry. This device supplies a power conversion efficiency of 0.9% with a very large open circuit voltage of 0.98 V. Very interestingly, conductivity measurements, performed by flash photolysis time-resolved microwave method (FP-TRMC), evidence that CS-COF is one of the best hole-transporting organic semiconductors ever reported having a hole-conducting mobility of 4.2 $cm^2 \cdot V^{-1} \cdot s^{-1}$. Bein and co-workers successfully obtained thiophene-based COF (TT-COF) to be implemented in a photo-voltaic device by co-condensing thieno-[3,2-b]-thiophene-2,5-diyldiboronic acid (TTBA) and hexa- hydroxytriphenylene (HHTP) [186]. They prepared a thin film COF that was employed as photoactive material to produce a photovoltaic cell (i.e., ITO/TT-COF:PCBM/Al) with an overall efficiency up to 0.05% (OCV = 0.62 V). As a result, designing a COF with larger pores and better packing of PCBM into the pores should raise the photoconversion efficiency and assure a better charge transfer [187]. Similarly, Cheng and co-workers synthesized a COF by condensing (2,3,9,10,16,17,23,24-(octahydroxyphthalocyanito) zinc ($ZnPc[OH]_8$) with a blend of BDBA or a BDBA-derivative that included a pendent azide moiety (N3-BDBA), they inserted covalently-bonded C60 units within the COF pores and proved that the charge was effectively transferred [188]. Bein et al. reported on the synthesis of an oriented thin COF film containing benzodithiophene units and loaded with C60. The synthesis was carried out by co-condensing benzo[1,2-b:4,5-b']dithiophene-2,6-diyl diboronic acid (BDTBA) and HHTP under solvothermal conditions onto an ITO-coated glass substrate. Then two different solutions (i.e., [60] PCBM and [70] PCBM) were spin coated onto the COF-modified electrode. Thin BDT-COF films presented two important optical absorbance bands in the UV spectral region. Furthermore, the oriented BDT-COF films played a host role for different fullerene-based acceptors molecules. The photoluminescence of the BDT-COF film resulted to be quenched when these acceptors were loaded into COF and this evidence confirmed that charge transfer is taking place [189].

Covalent organic frameworks are also synthetized as donor-acceptor building blocks; the obtainment of such COFs with a good crystallinity degree is highly challenging. Indeed, a high crystallinity diminishes the occurrence of internal charge recombination that is detrimental for the photoconductive features of the material. Jiang and co-workers successfully obtained COFs made by columnar arrays of D-A blocks that exhibited vertically ordered p-n heterojunction leading to a remarkably enhanced photoconductivity without any additional dopants, as reported in Figure 11 [190].

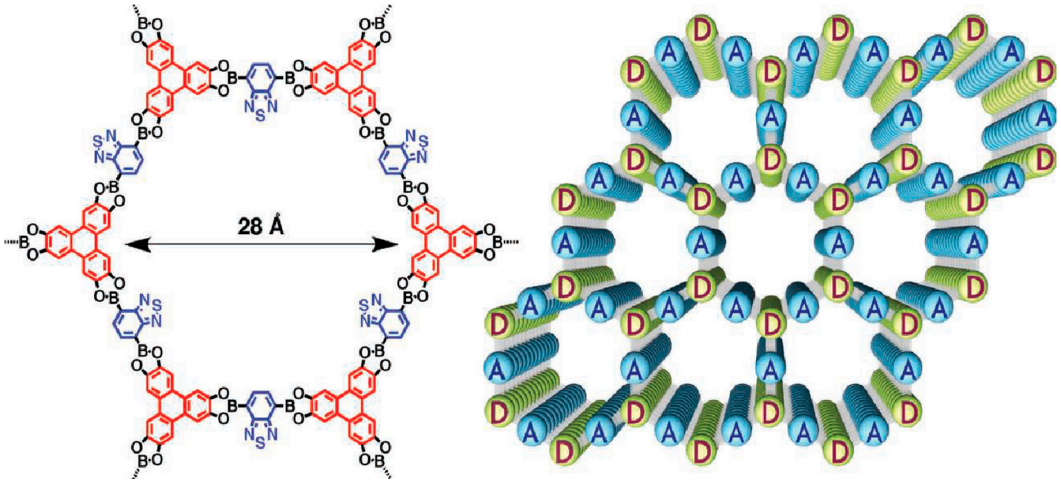


**Figure 11.** Schematic representation of 2D D-A COF with self-sorted and periodic electron donor-acceptor ordering and bicontinuous conducting channels (**right**: structure of one hexagon; **left**: a 3 × 3 grid). Reproduced with permission from [190].

Another donor-acceptor COF was obtained by Jin and co-workers. They synthesized DZnPc-ANDI-COF, based on zinc phthalocyanine as donor and naphthalene diimide as acceptor [191]. They also reported the substitution of the central metal ion, i.e., Zn, Cu or Ni to compare the physical properties of the different COFs [192]. When Zn is replaced by Cu or Ni the acceptor unit is still stable, and the charge separation lifetimes were very similar, even if the meta nature influenced the charge lifetimes. The copper-based COF achieved the longest lifetime, i.e., up to 33 µs. These results evidence how the thoughtful choice of the metal is a key parameter in the design of an effective D-A COF. In Table 4, the most effective COFs implemented in DSSCs are summarized.

**Table 4.** COFs effectively employed in DSSC. The reported values of photoconversion efficiency could not be compared between each-others, yet they could shine light on the potentiality of this class of material.

| Role | COFs | | η (%) | Ref. |
|---|---|---|---|---|
| | Name | Building Blocks | | |
| **Photoactive Material** | PPy-COF (Hexagonal) | 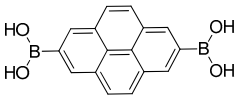 | n.a. | [180] |
| **Photoactive Material** | Metallophthalocyanine-COF (Tetragonal) | 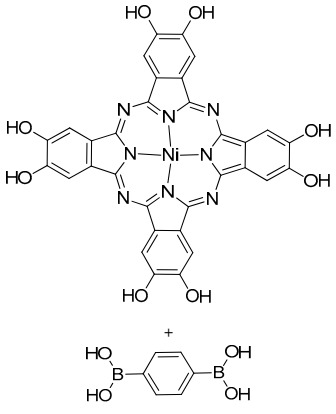 | n.a. | [181] |

**Table 4.** *Cont.*

| Role | COFs | | η (%) | Ref. |
|---|---|---|---|---|
| | Name | Building Blocks | | |
| **Photoactive Material** | NiPc-PBBA COF (Tetragonal) | 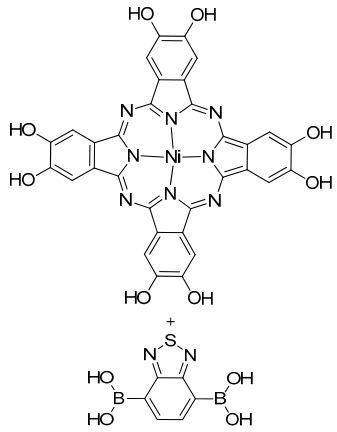 | n.a. | [182] |
| **Photoactive Material** | MP-COF (M = $H_2$, Zn, Cu) | 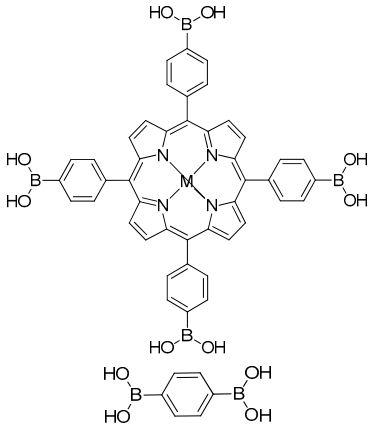 | n.a. | [183] |
| **Photoactive Material** | TP-COF, NiPBBA COF | 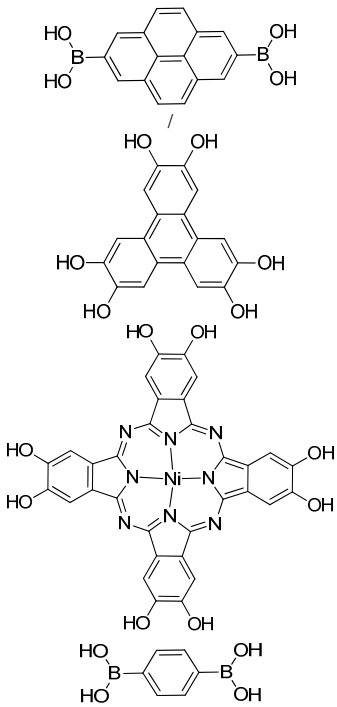 | n.a. | [184] |

**Table 4.** *Cont.*

| Role | COFs | | η (%) | Ref. |
|---|---|---|---|---|
| | Name | Building Blocks | | |
| **Photoactive Material** | CS-COF/$C_{60}$ (Hexagonal) | 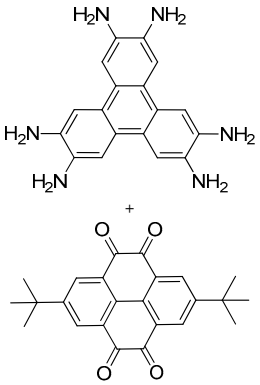 | n.a. | [185] |
| **Photoactive Material** | TT-COF:PCBM (Hexagonal) | 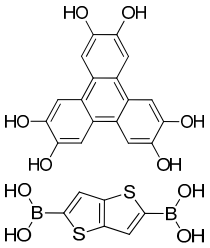 | 0.05 | [186] |
| **Photoactive Material** | [$C_{60}$]y-ZnPc-COFs | 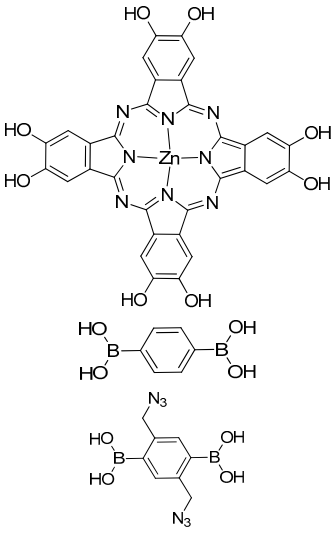 | n.a. | [188] |
| **Photoactive Material** | BDT-COF:[60]PCBM | 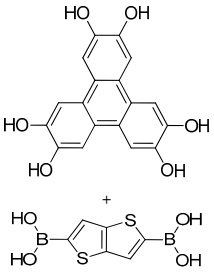 | n.a. | [189] |

**Table 4.** *Cont.*

| Role | COFs | | η (%) | Ref. |
|---|---|---|---|---|
| | Name | Building Blocks | | |
| **Photoactive Material** | D-A COF (Hexagonal). | 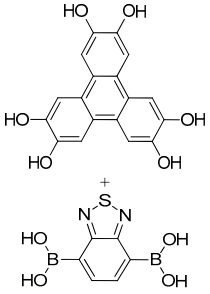 | n.a. | [190] |
| **Photoactive Material** | DZnPc-ANDI-COF | 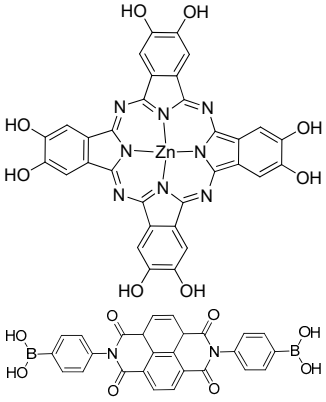 | n.a. | [191] |
| | DZnPc-ANDI-COF<br>DTP-APyrDI-COF | 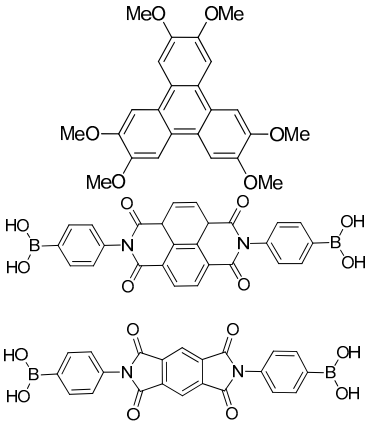 | n.a. | [193] |
| **Photo electrode** | triphenylene–porphyrin COF (Hexagonal), | 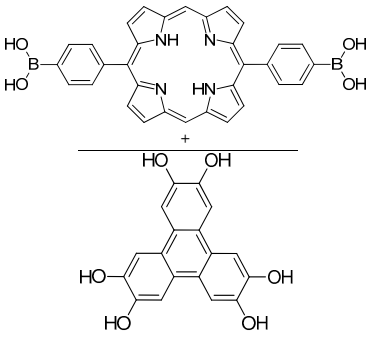 | n.a. | [194] |

Very interestingly, Jin et al. reported on a metal free D-A COF system [193]. More in details, they produced COF embodying triphenylene as a donor group and naphtaline diimide (DTP-ANDI-COF) or pyrromellitic diimide (DTP-APyrDI-COF) as acceptor. They investigated

fluorescence lifetimes by using time-resolved fluorescence spectroscopy and a value of 0.92 and 1.0 ns was measured for DTP-ANDI-COF and DTP-APyrDI-COF, respectively. Unfortunately, the induced photocurrent measured was null. This evidences how the presence of a metal atom is still required to obtain good photo-electrochemical responses. COF was employed as a photoactive layer in a photovoltaic cell by Calik and co-workers. They obtained a TP-Por COF by co-condensation reaction between bis(boron-phenyl)porphyrin and HHTP [194]. The so-obtained COF presented segregated donor and acceptor columns in which electrons and holes can move throughout the columns of porphyrins and HHTP, respectively. A thin film of TP-Por COF was grown on an ITO substrate, then a 20 nm thick coating of ZnO nanoparticles was spin-coated over it, being Al the counter electrode. Even if they observed very low photoconversion; this work evidenced that COFs are promising candidates for the photovoltaics application in the forthcoming.

## 3. Perovskite Solar Cells (PSCs)

In the last five years, organic–inorganic hybrid perovskite solar cells (PSCs) have gained great attention thanks to their high cell efficiency exceeding 20% [195–198]. PSCs are multilayer devices in which the perovskite film (behaving as light-harvester) is sandwiched between an electron transporting layer (ETL) and a hole transporting layer (HTL). In a n-i-p geometry the ETL (usually mesoporous or compact $TiO_2$) also acts as substrate for the deposition of the perovskite film. The HTM (e.g., a (un)doped organic polymer) is then deposited onto the PSK film and the device is finished with a metallic contact (Au, Ag . . . ) as shown in Figure 12 [199,200].

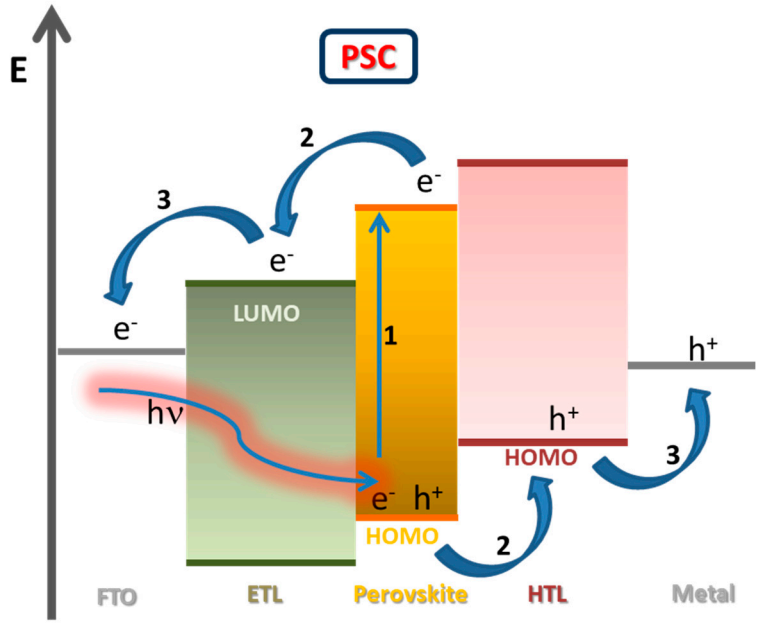


**Figure 12.** Band diagram and main processes and PSC: (1) Absorption of photon and free charges generation; (2) Charge transport; (3) Charge extraction.

The general formula of hybrid perovskite formula is $ABX_3$ in which A is methyl ammonium or another monovalent cation, B is Pb (II) or Sn (II), and X is $Cl^-$, $Br^-$, or $I^-$. If lead is the bivalent cation, methyl ammonium the monovalent cation and $I^-$ the anion, we obtain a methylammonium lead iodide perovskite ($MAPbI_3$). In this material, the orbitals of lead and iodine contributes to the energetic level of the PSK (HOMO and LUMO) whereas the methylammonium cation does not give any contribution to the electronic properties of the absorbing layer, being involved in the establishment of the 3D network of the crystal, though. Straightforwardly, MA deeply influences the optical properties of the PSK layer. $MAPbI_3$, and more broadly PSKs, has a direct bandgap of around 1.55 eV (absorption

onset of about 800 nm) and large absorption coefficient in the visible range. So, this generates a high density of photoexcited charges and assures efficient light-harvesting [201,202].

Perovskite solar cells are moderately cheap to produce (considering a low waste of materials in the scaling up) and can reach photoconversion efficiency comparable as those of commercially available silicon-based devices [5,203–207]. Indeed, their efficiency has rapidly raised from 3.8% [208] in 2009 to 23.3% in 2018 in single-junction architecture and to 27.3% in silicon/PSK tandem devices [5] being the latter more efficient than single junction counterparts. Indeed, perovskite solar cells are the fastest-growing solar technology up to today [209]. The possibility of creating low cost, thin, high efficiency, lightweight and flexible solar cells make them really fascinating.

Despite their major advantages, some issues could partially prevent the large-scale production of this class of solar cells: the use of lead is being debated today due to its toxicity and environmental harmfulness; the poor stability in the atmosphere due to degradative interaction with both oxygen and water and the partial photothermal instability of the perovskite layer itself [210]. In this context, the optimization of the ETL layer and its interface with perovskite film is of great importance to ameliorate the photostability of the device. Among different strategies [211], the employment of MOF-modified ETL could be a low-cost and feasible route. Three-dimensional perovskite structures consisted of highly porous $TiO_2$-MOF that have many advantages such as high stability, fast charge carrier, and high absorption coefficient [212] leading to the obtainment of photoactive ETLs. Up to now, just few examples of implementation of metal organic frameworks in PSCs have been reported. In the following subsection we briefly review them.

### *3.1. MOFs in PSCs*

Vinogradov and co-workers implemented, for the first time, a crystalline metal-organic framework, namely MIL-125 ($Ti_8O_8(OH)_4$-$(O_2C$-$C_6H_4$-$CO_2)_6$, as an active material in a perovskite solar cell [213]. They performed a single-step synthesis to obtain a $TiO_2$-MOF composite during which water was added as a limiting reactant for $Ti(OC_3H_7)_4$ causing a step-by-step growth of a hetero-phasic system. Initially, a titanium oxyhydroxide precipitate was formed and then it was converted into crystalline anatase by a hydrothermal treatment. By varying the initial concentration of precursor the MOF content in $TiO_2$ was tuned, being at least 5% w/w. The solid compound was washed twice with methanol and dried at 200° C before being employed as ETL in a PSC. 3% MOF-modified $TiO_2$ was found to be the most efficient ETL, leading to a 6.4% photoconversion efficiency (being $FAPbI_3$ the PSK layer). The band gap of commercial $TiO_2$ is approximately 3.3 eV that could cause problems in exciting and injecting the electrons, which gives rise to inefficient electron transportation and then poor electrical conductivity. To improve the latter, Nguyen and Bark reported on the doping of $TiO_2$ with Co-metal organic framework by solvothermal method [214]. They obtained a PCE close to 16% by employing 1 wt% Co-doped $TiO_2$ shifting the band gap low to 2.4 eV.

High crystallinity and proper morphology are two key parameters to obtain efficient PSCs; up to now, the deposition methods to obtain the wanted features are quite expensive, time-demanding and they required numerous synthetic steps [215–218]. To overcome these issues, Chang et al. tried to increase the crystallinity of PSK layer by embedding the latter in a MOF nano-crystalline (140 nm) matrix by using just one deposition step [219]. More in detail, they use a Zn-based MOF (i.e., MOF-525) [220] with a cubic structure to incorporate the perovskite crystals by driving a more efficient and homogeneous crystallization process. Once implemented in a complete PSCs, they obtain an overall conversion efficiency up to 12%. They performed chronoamperometric experiments to figure out the reason the difference in redox activity of the MOF-525 and metal-based MOF-525 thin films proving that the apparent diffusion coefficient ($D_{app}$) of the Zn-MOF-525 thin film is higher than that of the Co-MOF-525 thin film. Moreover, Co-MOF-525 thin film obtains higher $D_{app}$ than the MOF-525 thin film. As a result, it is observed that the Zn-MOF-525 thin film supplies faster charge hopping or faster ion diffusion compared to the Co-MOF-525 and MOF-525 thin films.

Li et. al. presented for the first time ZIF-8 in DSCCs customizing the surface of a $TiO_2$ electrode and they succeeded to enhance the open-circuit voltage [93]. More recently, also used ZIF-8 in PSCs trying to correlate the quality of the MOF layer at the interface between ETL and PSK and the photovoltaic performance [221]. A thin interlayer of ZIF-8 was coated on the surface of mesoporous-$TiO_2$ (mp-$TiO_2$) to control the growth of a perovskite crystalline layer. When ZIF-8 was employed as additional layer at the interface between mp-TiO2 and the perovskite film, they obtain a substantial improvement of both crystallinity and morphology of the perovskite thin film that lead to a PCE close to 17% and higher than reference performances. PCE for the PSC with pure mp-$TiO_2$ as the ETL was 14.75% ($J_{SC}$ of 20.77 mA $cm^2$, $V_{OC}$ of 1.00 V, FF of 0.71). On the other hand, the device with the ZIF-8-20 interfacial layer reached a better efficiency of 16.99% ($J_{SC}$ of 22.82 mA $cm^2$, $V_{OC}$ of 1.02 V, FF of 0.73). A similar approach to enhance optical harvesting and electron extraction efficiency was recently reported by Zhang and co-workers, introducing a MOF-derived ZnO (MZnO) with dodecahedron porous structure, namely ZIF-8 [222]. The introduction of MOF-derived ZnO as ETL allows to reach more efficient electron extraction and to reduce trap state density leading to a lower electron-hole recombination. Thus, higher fill factor (0.74) and short-circuit current density (22.1 mA $cm^2$) were achieved (PCE = 18.1%). When comparing the effect of different sizes of M-ZnO on the performance of perovskite films and PSCs, the optimum was reached for a MOF particle size of about 120 nm. Additionally, the so-obtained devices showed almost no hysteresis effect, and performance attenuation in the ambient atmosphere over time was eliminated.

Oriented microporous metal−organic framework (MOF) thin films made through a liquid phase technique for $CH_3NH_3PbI_2X$ (X = Cl, Br, and I) perovskite was reported by Chen et al. [223]; $PbI_2$ and $CH_3NH_3X$ (MAX) precursors were introduced into MOF HKUST-1 ($Cu_3(BTC)_2$, BTC = 1,3,5-benzene tricarboxylate) thin film and allowed to crystallize in order to obtain extra small $MAPbI_2X$ (X = Cl, Br, and I) quantum dots with a diameter lower than 2 nm (i.e., comparable with the dimensions of the micropores in the MOF structure). The so-obtained hybrid structure was found to be quite irresponsive to air exposure having high stability. Unfortunately, the authors did not report the implementation of this PSK layer into a complete device. It is worth mentioning that just few studies about incorporation of MOFs into perovskite solar cells have been published so far. One of these studies reports on the implementation of an In-based MOF, i.e., $[In_2(phen)_3Cl_6]\cdot CH_3CN\cdot 2H_2O$ (namely In2), as hole transport material in PSCs. Its implementation allowed to finely tune the band alignment between the energy levels of PSK and HTM. Straightforwardly, the authors enhanced short-current density (from 19.53 to 21.03 mA $cm^{-2}$), open circuit voltage (from 0.98 to 1.10) and FF (from 0.67 to 0.74) in comparison with reference devices leading to a significant increase in the cell efficiency from 12.8% to 15.8% [224]. The authors ascribed these unexpected results to both a decrement in the concentration of pin holes in the HTM and an increase in the light absorption of the device assured by the In2 behaving as a scattering layer. Additionally, the emission spectra of the employed MOF are partially superimposed to the absorption profile of the perovskite.

In order to obtain flexible but high performing PSCs, the nanometric $TiO_2$ particle should be replaced by ultra-small ones that should require relatively low sintering temperature to not damage the flexible substrate (usually made of PET/ITO, with the polymeric substrate being unstable above 120 °C).

In this context, Ti-based MOFs could be effectively employed being well-ordered materials constituted by Ti-oxo clusters and organic linkers [48,225]. Ryu and co-workers used nanocrystalline nTi-MOF (ca. 6 nm) as ETL in PSCs [226]. This MOF was proved to effectively assure the electrons transport throughout the ETL. Remarkably, the embodiment of PCBM into the MOF matrix further enhanced the film conductivity. Perovskite solar cells made by nTi-MOF showed good photoconversion efficiency both in rigid and flexible architecture, 18.9% and 17.4%, respectively. Very interestingly, the stability of the device was maintained after more than 700 bending cycles (i.e., 15.4%, 0.88 of its initial value). Therefore, this approach could be very promising to obtain flexible, efficient and stable PSCs.

Zhao et al. employed the same MOF (MIL-125) as ETL [227]: they obtained cakelike nanocrystals leading to a better crystallization of the perovskite film and reducing, in turns, the electron-hole pair recombination. The relative devices reached a PCE close to 13% and almost null hysteresis. The efficiency of perovskite/Zr-based MOF heterojunction in PSCs were investigated by means of two types of Zr-MOFs, and UiO-66 and MOF-808 was selected as a MOFs combination because of their chemical and moisture durability [228]. When MOFs were used as an interlayer (deposited onto the ETL one before the growth of the PSK layer) they drove the growth of the perovskite layer leading to a better crystallinity. UiO-66/MOF-808-modified PSCs exhibited power conversion efficiencies up to 17.0% and 16.6%, outperforming the control device (15.8%). Furthermore, both MOFs partially acted as UV-filters leading to a better photostability of the device. Indeed, the hybrid MOFs distribute over the perovskite grain boundary contributing a grain-locking effect to simultaneously passivate the defects and to strengthen the film's durability against moisture invasion. Over 70% of the initial PCE was maintained after being stored in air (25° C and relative humidity of 60 ± 5%) for over 2 weeks. In Table 5, the most effective COFs implemented in PSCs are summarized.

**Table 5.** Metal-organic frameworks implemented in perovskite solar cells. For sake of brevity, we prefer to report the metal and the organic linker separately. The reported values of photoconversion efficiency could not be compared between each-others, yet they could shine light on the potentiality of this class of material. The main role of the MOF is bold in the first column.

| Role | MOFs | | η (%) | Ref. |
|---|---|---|---|---|
| | Metals | Organic Linker(s) | | |
| **Photoactive Material** | Ti | MIL-125(Ti) 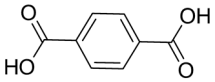 | 6.4 | [213] |
| **Photoactive Material** | Zr | MOF-525 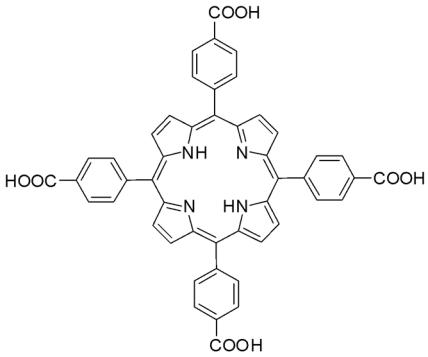 | 12 | [220] |
| **Photoactive Material** | Zn | ZIF-8  | 16.99 | [221] |
| **Photoactive Material** | Cu | HKUST-1 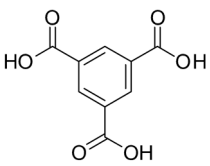 | n.a. | [223] |

**Table 5.** *Cont.*

| Role | MOFs | | η (%) | Ref. |
|---|---|---|---|---|
| | Metals | Organic Linker(s) | | |
| **Hole Transport Material (HTM)** | In | 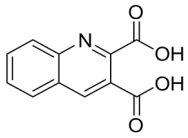 | 15,8 | [225] |
| **Electron Transport Layer (ETL)** | Ti | MIL-125(Ti) 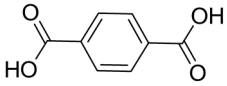 | 18.9 | [226] |
| **Electron Transport Layer (ETL)** | Zr | UiO-66, MOF-808 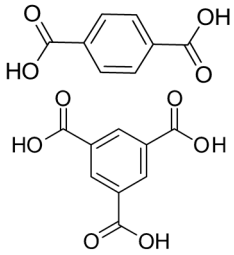 | 17 | [228] |
| **Hole Transport Material (HTM)** | In | 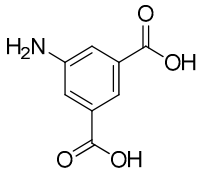 | 18.51 | [207] |
| **Hole Transport Material (HTM)** | In | 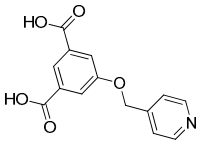 | 19.47 | [208] |

As one can see from Table 4, MIL-125 was employed in both the photoactive material [213] and in the ETL [226]. This is a meaningful proof of the versatility of metal-organic frameworks. It is worth mentioning that just few works have been presented on the implementation of MOFs in perovskite solar cells; yet, the photoconversion efficiency reached is very promising and there is plenty of room for implementation.

In the last few years, growing attention was dedicated to the employment of MOFs and MOF-derivatives as doping agents to enhance the performances and the stability of conventional HTM, namely SPIRO-o-MeTAD. Aiming at this, the first attempts were made with indium-based MOFs: in 2019, Yang et al. reported In10 ($[In_{0.5}K_{(3\text{-}qlc)}Cl_{1.5}(H_2O)_{0.5}]_{2n}$) as an effective oxidative host for SPIRO-o-MeTAD leading to a higher conductivity of the HTL and suppressing charge recombination at the interface with PSK [229]. As an added property, In10 increased the light response of PSCs due to its photoluminescence properties: this led to an overall efficiency of 17% ($J_{SC}$ = 24.3 mA $cm^{-2}$, $V_{OC}$ = 1 V, FF = 0.7). A parallel approach was proposed by the same group [230]: they employed In-Aipa, $[In(Hipa\text{-}NH_2)_2$ $(ipa\text{-}NH_2)_2]\cdot 5H_2O$, a 2D indium-based MOF as an effective auxiliary additive (in conjunction with both Li-TFSI and TBP that are very useful to increase the quality of HTM but jeopardize the long-term stability of the device) in SPIRO-o-MeTAD [231,232]. The resulting devices reached a PCE close to 19% and, more remarkably, they retained over 85% of the initial PCE after 720 h of air exposure. This result can be promising in terms of highly efficient and long-term stable PSC devices. A further step toward more stable PSCs was made by the same group through the replacement

of TBP with a different In-based MOF, namely In(HPyia)$Cl_2$]·$CH_3CN$ (In-Pyia) [233]. As a matter of fact, TBP, which is highly volatile liquid phase component, caused the aggregation, hydration, and ion penetration of lithium salts into the PSK layer. The In-Pyia-modified PSCs boosted power conversion efficiency up to 20% surpassing the typical devices including t-BP (18%). In addition, In-Pyia-based device achieved a longer stability if compared with the TBP-based counterpart maintaining 81% of the initial PCE after 16 days without any encapsulation (below 20% for control device).

The examples analyzed above employed In-based MOFs. Other approaches involved lead [234] and copper-based [235] materials. Zeng et al. combined a 2D Pb-based MOF with Spiro-OMeTAD as innovative HTL in PSCs [234]. The authors evidenced a haloing orienting effect of the latter leading to a smoother interface with PSK, higher hydrophobicity and an upshifting of the energy level when compared to Spiro-O-MeTAD, leading to a 25% increase in PCE and a longer stability. Instead, Cu-based MOF was employed by Fan's group who proposed the first application of hybrid material as oxidant in the HTM layer [235]. They tested a hybrid polyoxometalate@metal–organic framework (POM@MOF) material, $[Cu_2(BTC)4/3\text{-}(H_2O)_2]_6[H_3PMo_{12}O_{40}]_2$ for the oxidation of spiro-OMeTAD with Li-TFSI and TBP. POMs began to attract attentions in PSCs, owing to their strong electron-accepting and oxidation ability, [236] being able to oxidize spiro-OMeTAD in an inert condition, and increase conductivity and performance of device [237]. In this context, POM@Cu-BTC composite showed dual-functions during chemical doping spiro-OMeTAD increasing the hole mobility of the resulting HTM by a factor of 2 and an overall PCE close to 22%.

### *3.2. COFs in PSCs*

Initially, researchers' efforts were focused on obtaining and implementing 2D COFs whereas more recently 3D COFs have also shown some interesting features. Concerning emerging photovoltaics, Wu et. al. has recently reported highly conjugated three-dimensional COFs based-on spirobifluorene and their employment in perovskite solar cells [238]. They employed these COFs as an additive into the perovskite layer. They obtained 3D ordered porous frameworks with an orthogonal configuration of biplanar spirobifluorene units as tetrahedral nodes. This structure presented several electron-transporting channels in the frameworks with highly ordered array by having rigid and long-range conjugated systems. When a SP-3D-COFs-mdified PSK layer was used in a complete device led to a power conversion efficiency up to 18.3% for SP-3D-COF 1 and 18.7% for SP-3D-COF 2 that are extremely higher if compared to reference device (PCE = 15.8%). More recently, Kuo et al. used 2D-COF based on a building block of tetraphenylethylene as a hole transport layer for the modification of both PTAA or NiO in inverted perovskite solar cells [239]. In the case of PTAA-based PSCs, the establishment of π–π interactions between COF and the HTL led to an amelioration of the photoconversion efficiency, approaching 20% (Figure 13). Furthermore, the presence of COF interlayer seems to improve both the crystallinity and the morphology of the perovskite layer.

A new approach for synthesis of 2D imine-based COFs was reported by Li et al. [240]: pyrene units, containing two different functional groups which are formyl and amino groups, were used and polymerized through self-assembly condensation reaction. They also obtained pyrene-COFs using two different pyrene units by co-condensation reactions. The former approach allows to obtain COFs exhibiting higher crystallinity as well as higher porous surface (BET Surface; 1200–1372 $m^2/g$). This is actually a promising strategy to obtain COFs in a mild condition. This pyrene-COF was also used as a HTLs combining with PTAA in PSCs reaching a photoconversion efficiency as high as 6.36% ($V_{OC}$ of 0.76 V, $J_{SC}$ of 15.4 $mA/cm^2$, and a FF of 54%).

As far as we are aware, these are the only examples regarding the effective implementation of a covalent organic framework in perovskite solar cells. Yet, following on from the extremely good photoconversion efficiency, it could soon become the milestone for future improvements in this field. We are quite confident that the best is yet to come!

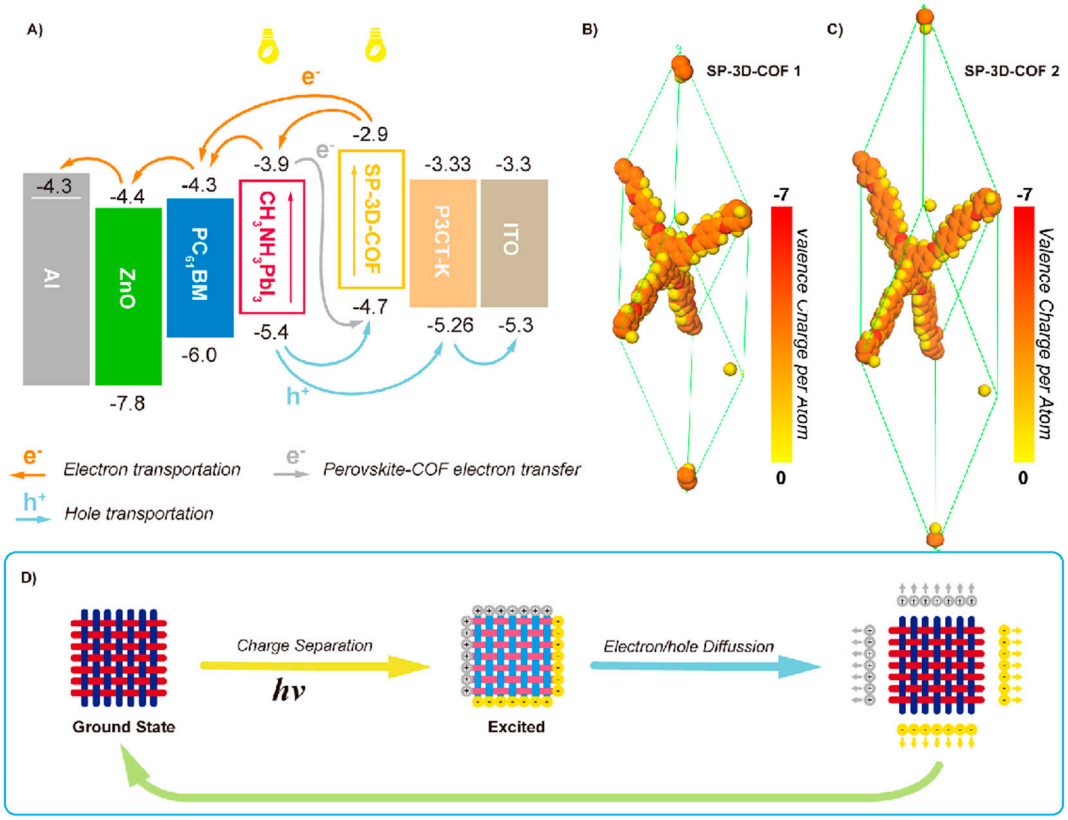


**Figure 13.** Interplay between the COF layer and other component of PSCs stack. (**A**) Schematic energy level diagram of SP-3D-COFs doped PSCs with energy levels of SP-3D-COFs calculated from plane-wave DFT; (**B**,**C**) geometry optimized framework from the plane-wave DFT calculations of (**B**) SP-3D-COF 1 and (**C**) SP- 3D-COF 2; (**D**) proposed mechanism of photoinduced charge separation. Reproduced with permission from [239].

## 4. Conclusions

Throughout the present review, we discuss on the implementation of both metal-organic frameworks (MOFs) and covalent organic frameworks (COFs) in emerging photovoltaics, namely dye-sensitized solar cells (DSSCs) and perovskite solar cells (PSCs). Both MOFs and COFs have a unique structure with a great tunability of their organic and inorganic components that confer incredible chemical versatility. For this reason, they can be used in many areas: from capture, storage, separation, and conversion of gases to (photo)catalysis and drug delivery, from optoelectronic to sensors, and from magnetism and ferroelectricity to light harvesting and energy transfer. As far as the photovoltaic field is concerned, they do not have a unique role but, based on their photophysical and chemical properties, they could be effectively employed as photoactive material, electrodes or charge carriers, accomplishing mainly all the single components of a PV device. So, we do not feel to propose new applications but the main idea that should come out from this review is that there is still a large space for the implementation of the single PV device component with MOF- and COF-based materials (in particular as photoactive material or as hole transporting material in PSCs or photoanodic material or solid-state sensitizers in DSSCs). Indeed, based on their photophysical and chemical properties, they could be effectively employed as photoactive materials, electrodes or charge carriers. Indeed, MOFs are complex materials with highly tunable properties that could be largely exploited in order to design tailored features. Actually, MOFs can play different roles in a DSSC being able to act as photosensitizers, electrolyte additives or electrode materials. When employed as electrode-modifier and/or interlayer, MOFs have demonstrated to improve the dye loading thanks to their wide surface area and high porosity. Moreover, they are very good candidates as photoelectrode

materials since, due to their electrical insulating properties, they can effectively minimize the interfacial charge recombination between the electrolyte and the electrons injected in the conduction band of $TiO_2$. The highest efficiency reached is over 7% when MOF was used as photoanode exploiting the excellent ability to increase scattering capacity of incident light as well as demonstrating low loss ratio of photogenerated electrons by small dark current. The light harvesting capacity of MOFs can be easily tuned by choosing the appropriate organic linker, extending the absorption region within the ultraviolet and blue-violet region of the solar cells. The best overall efficiency is above 8% for a liquid-junction DSSC employing Indium(III)–Potassium(I) Metal–Organic Framework as a sensitizer in combination with N719. Some recent examples also report the use of MOFs as photosensitizers in solid-state photovoltaic cells. Another possible role of MOFs is their use as counter-electrode in order to reduce the cell costs getting rid of Pt. The preliminary results reported so far are very promising with overall photoconversion efficiency up to 9% due to large surface area and good electronic properties, i.e., an easier diffusion of iodine-based redox couple. In particular, it is worth noting that MOFs could be directly used as counter-electrode in place of Pt and could be seriously investigated as an effective low-cost and feasible alternative to platinum as counter-electrodes in DSSCs. A different, but somehow complementary, approach consists in the employment of custom-made MOFs as precursors to obtain, by thermal decomposition, a counter-electrode with specific properties and morphology (usually metal sulphides and oxides are obtained by this approach).

The high versatility of MOFs is even more evident in the different roles they can fill in PSCs: indeed, they could be effectively applied as photoactive material, HTM or ETL. In all the reported cases, the photoconversion efficiency reached, still remaining well below the state of the art, demonstrates the great possibilities in the implementation of the final device. The use of MOF as electron transport layer can enhance optical harvesting and electron extraction efficiency reducing the trap state density leading to a lower electron-hole recombination. In addition, the MOF-based devices showed almost no hysteresis effect and improved stability. The same turned out to be true when MOF is employed as doping agent for conventional HTMs. The overall efficiency is above 19% with remarkable stability.

On the other side, the specific role of covalent organic frameworks in DSSCs and PSCs is still not very clear since very few examples are present in the literature. Most of the studies reported on the possible implementation of COF structures in emerging PV but they mainly investigate their photoelectrochemical properties without showing their use in a real device. Some examples concern the use of COFs in PSCs with efficiency exceeding 18% where the presence of COFs seemed to improve both the crystallinity and the morphology of the PSK layer. These few examples are in any case very promising results for an effective implementation of COFs in PSCs.

**Supplementary Materials:** The following are available online at http://www.mdpi.com/1996-1073/13/21/5602/s1, Figure S1: Basic topological diagrams for the design of 2D and 3D COFs, Table S1: Photovoltaic parameters of most efficient MOF- and COF-based devices.

**Author Contributions:** Conceptualization, N.B., F.B. and C.B.; resources, B.C., F.B., G.V. and C.B.; data curation, M.B. and N.B.; writing—original draft preparation, O.Y. and M.B.; writing—review and editing, O.Y., M.B., N.B., C.A. and G.V.; visualization, O.Y. and C.A.; supervision, N.B. and C.B.; project administration, B.C., F.B. and C.B.; funding acquisition, B.C. All authors have read and agreed to the published version of the manuscript.

**Funding:** The authors acknowledge a grant of the Department of Chemistry of University of Turin on "Harnessing the power of light in photoactive metal-organic frameworks" within the initiative denoted "Tomorrows" to promote the collaboration among research groups.

**Conflicts of Interest:** The authors declare no conflict of interest.

## Abbreviations

| | |
|---|---|
| 3D | 3-Dimensional |
| ACN | Acetonitrile |
| BDBA | 1,4-Benzenediboronic acid |
| BDBA | 1,4-Benzenediboronic acid |
| CE | Counter-electrode |
| CNR | Carbon nanorode |
| COF | Covalent organic framework |
| DAPV | Diaminopropyl viologen |
| DEF | Diethylformamide |
| DSSC | Dye-sensitized solar cells |
| DTP-ANDI | Naphtaline diimide |
| DTP-APyrDI | Pyrromellitic diimide |
| EIS | Electrochemical impedance spectroscopy |
| ETL | Electron transporting layer |
| FF | Fill factor |
| FP-TRMC | Flash photolysis time resolved microwave method |
| FTO | Fluorine-doped Tin Oxide |
| $H_4$DOBDC | 2,5-Dihydroxyterephthalic acid |
| HHTP | 2,3,6,7,10,11-Hexahydroxytriphenylene |
| HHTP | 2,3,6,7,10,11-Hexahydroxytriphenylene |
| HOMO | Highest occupied molecular orbital |
| HTL | Hole transporting layer |
| HTM | Hole transport materials |
| ITO | Indium tin oxide |
| $J_{SC}$ | Short circuit photocurrent |
| LED | Light emitting electrochemical diodes |
| LEEC | Light emitting electrochemical cells |
| LDH | Layered double hydroxide |
| LUMO | Lowest unoccupied molecular orbital |
| MOF | Metal-organic framework |
| MPN | 3-Methoxypropionitrile |
| MW | Microwave |
| MWCNT | Multi-walled carbon nanotube |
| $NH_2$-bdc | 2-Aminoterephthalic acid |
| NiPc-BTDA | Nickel phthalocyanine-3,3′,4,4′-benzophenonetetracarboxylic acid dianhydride |
| NIR | Near infrared |
| NMP | N-Methyl-2-pyrrolidone |
| NP | Nanoparticle |
| NT | Nanotube |
| OPV | Organic photovoltaic |
| PBBA | 1,4-Phenylenebis(boronic acid) |
| PCBM | Phenyl-$C_{61}$-butyric acid methyl ester |
| PCE | Power conversion efficiency |
| PCP | Porous coordination polymer |
| PEDOT | Poly(3,4-ethylenedioxythiophene) |
| PEGDGE | Poly(ethylene glycol) di-glycidyl ether |
| PET | Polyethylene Terephthalate |
| PMMA | Poly(methyl methacrylate |
| PPF | Pillared porphyrin framework |
| PPy | Polypyrrole |
| PSC | Perovskite solar cell |
| PSK | Perovskite |
| PT | *tert*-Butylpyrenetetraone |

| | |
|---|---|
| PVs | Photovoltaics |
| QD | Quantum dot |
| QSDSSC | Quasi-solid dye-sensitized solar cells |
| RT | Room temperature |
| RGO | Reduced graphene oxide |
| SC | Solar cell |
| SLG | Single-layer graphene |
| SP | Spirobifluorene |
| SURMOF | Surface-anchored metal-organic framework |
| TBP | *tert*-Butylpyridine |
| TCO | Transparent conductive oxide |
| TPHA | Triphenylene hexamine |
| TTBA | Thieno-[3,2-b]-thiophene-2,5-diyldiboronic acid |
| UV | Ultraviolet |
| $V_{OC}$ | Open-circuit voltage |
| ZIF | Zeolitic imidazolate framework |
| $ZnPc[OH]_8$ | 2,3,9,1016,17,23,24-(Octahydroxyphthalocyanito) zinc |
| Zn-TCPP | Zinc(II) meso-tetrakis(4-carboxyphenyl)porphyrin |
| η | Power conversion efficiency |

## References


1. Grätzel, M. Photovoltaic and photoelectrochemical conversion of solar energy. *Philos. Trans. R. Soc. A Math. Phys. Eng. Sci.* **2007**, *365*, 993–1005. [CrossRef] [PubMed]
2. Meillaud, F.; Boccard, M.; Bugnon, G.; Despeisse, M.; Hänni, S.; Haug, F.-J.; Persoz, J.; Schüttauf, J.-W.; Stuckelberger, M.; Ballif, C. Recent advances and remaining challenges in thin-film silicon photovoltaic technology. *Mater. Today* **2015**, *18*, 378–384. [CrossRef]
3. Mehmood, H.; Tauqeer, T.; Hussain, S. Recent progress in silicon-based solid-state solar cells. *Int. J. Electron.* **2018**, *105*, 1568–1582. [CrossRef]
4. Chapin, D.M.; Fuller, C.S.; Pearson, G.L. A new silicon p-n junction photocell for converting solar radiation into electrical power. *J. Appl. Phys.* **1954**, *25*, 676–677. [CrossRef]
5. Alta, F.; Asu, E.S. National Renewable Energy Labs (NREL) efficiency chart. 2019. 2020. Available online: https://www.nrel.gov/pv/assets/pdfs/best-research-cell-efficiencies.20200925.pdf (accessed on 30 August 2020).
6. Shockley, W.; Queisser, H.J. Detailed balance limit of efficiency of p-n junction solar cells. *J. Appl. Phys.* **1961**, *32*, 510–519. [CrossRef]
7. Freitag, M.; Teuscher, J.; Saygili, Y.; Zhang, X.; Giordano, F.; Liska, P.; Hua, J.; Zakeeruddin, S.M.; Moser, J.-E.; Grätzel, M.; et al. Dye-sensitized solar cells for efficient power generation under ambient lighting. *Nat. Phot.* **2017**, *11*, 372–378. [CrossRef]
8. Wu, T.-C.; Long, Y.-S.; Hsu, S.-T.; Wang, E.-Y. Efficiency Rating of Various PV Technologies under Different Indoor Lighting Conditions. *Energy Procedia* **2017**, *130*, 66–71. [CrossRef]
9. Fakharuddin, A.; Jose, R.; Brown, T.M.; Fabregat-Santiago, F.; Bisquert, J. A perspective on the production of dye-sensitized solar modules. *Energy Environ. Sci.* **2014**, *7*, 3952–3981. [CrossRef]
10. McConnell, I.; Li, G.; Brudvig, G.W. Energy Conversion in Natural and Artificial Photosynthesis. *Chem. Biol.* **2010**, *17*, 434–447. [CrossRef]
11. Schulze, T.F.; Schmidt, T.W. Photochemical upconversion: Present status and prospects for its application to solar energy conversion. *Energy Environ. Sci.* **2015**, *8*, 103–125. [CrossRef]
12. Grätzel, M. Solar energy conversion by dye-sensitized photovoltaic cells. *Inorg. Chem.* **2005**, *44*, 6841–6851. [CrossRef] [PubMed]
13. Solanki, M.S.; Dangi, T.; Tak, P.; Sharma, S.; Ameta, R. Organic photovoltaic cells. *Sol. Energy Convers. Storage Photochem. Modes* **2015**, *10*, 55–84. [CrossRef]
14. Segura, J.L.; Martín, N.; Guldi, D.M. Materials for organic solar cells: The C60/π-conjugated oligomer approach. *Chem. Soc. Rev.* **2005**, *34*, 31–47. [CrossRef]
15. Wong, W.Y.; Ho, C.L. Organometallic Photovoltaics: A New and Versatile Approach for Harvesting Solar Energy Using Conjugated Polymetallaynes. *Acc. Chem. Res.* **2010**, *43*, 1246–1259. [CrossRef]

16. Cavallo, C.; Di Pascasio, F.; Latini, A.; Bonomo, M.; Dini, D. Nanostructured Semiconductor Materials for Dye-Sensitized Solar Cells. *J. Nanomater.* **2017**, *2017*, 5323164. [CrossRef]
17. Luceño-Sánchez, J.; Díez-Pascual, A.; Peña Capilla, R. Materials for Photovoltaics: State of Art and Recent Developments. *Int. J. Mol. Sci.* **2019**, *20*, 976. [CrossRef] [PubMed]
18. Zhou, H.-C.; Long, J.R.; Yaghi, O.M. Introduction to Metal–Organic Frameworks. *Chem. Rev.* **2012**, *112*, 673–674. [CrossRef] [PubMed]
19. Medina, D.D.D.; Sick, T.; Bein, T. Photoactive and Conducting Covalent Organic Frameworks. *Adv. Energy Mater.* **2017**, *7*, 1700387. [CrossRef]
20. Wu, S.; Li, Z.; Li, M.Q.; Diao, Y.; Lin, F.; Liu, T.; Zhang, J.; Tieu, P.; Gao, W.; Qi, F.; et al. 2D metal–organic framework for stable perovskite solar cells with minimized lead leakage. *Nat. Nanotechnol.* **2020**, in press. [CrossRef]
21. Chueh, C.C.; Chen, C.I.; Su, Y.A.; Konnerth, H.; Gu, Y.J.; Kung, C.W.; Wu, K.C.W. Harnessing MOF materials in photovoltaic devices: Recent advances, challenges, and perspectives. *J. Mater. Chem. A* **2019**, *7*, 17079–17095. [CrossRef]
22. Wu, X.-P.; Choudhuri, I.; Truhlar, D.G. Computational Studies of Photocatalysis with Metal–Organic Frameworks. *Energy Environ. Mater.* **2019**, *2*, 251–263. [CrossRef]
23. Nasalevich, M.A.; Hendon, C.H.; Santaclara, J.G.; Svane, K.; Van Der Linden, B.; Veber, S.L.; Fedin, M.V.; Houtepen, A.J.; Van Der Veen, M.A.; Kapteijn, F.; et al. Electronic origins of photocatalytic activity in d0 metal organic frameworks. *Sci. Rep.* **2016**, *6*, 23676. [CrossRef] [PubMed]
24. Stock, N.; Biswas, S. Synthesis of Metal-Organic Frameworks (MOFs): Routes to Various MOF Topologies, Morphologies, and Composites. *Chem. Rev.* **2012**, *112*, 933–969. [CrossRef]
25. Rubio-Martinez, M.; Avci-Camur, C.; Thornton, A.W.; Imaz, I.; Maspoch, D.; Hill, M.R. New synthetic routes towards MOF production at scale. *Chem. Soc. Rev.* **2017**, *46*, 3453–3480. [CrossRef] [PubMed]
26. Howarth, A.J.; Peters, A.W.; Vermeulen, N.A.; Wang, T.C.; Hupp, J.T.; Farha, O.K. Best practices for the synthesis, activation, and characterization of metal–organic frameworks. *Chem. Mater.* **2017**, *29*, 26–39. [CrossRef]
27. Geng, K.; He, T.; Liu, R.; Dalapati, S.; Tan, K.T.K.T.; Li, Z.; Tao, S.; Gong, Y.; Jiang, Q.; Jiang, D. Covalent Organic Frameworks: Design, Synthesis, and Functions. *Chem. Rev.* **2020**, *120*, 8814–8933. [CrossRef] [PubMed]
28. Li, Y.; Chen, W.; Xing, G.; Jiang, D.; Chen, L. New synthetic strategies toward covalent organic frameworks. *Chem. Soc. Rev.* **2020**, *49*, 2852–2868. [CrossRef]
29. Auras, F.; Ascherl, L.; Hakimioun, A.H.; Margraf, J.T.; Hanusch, F.C.; Reuter, S.; Bessinger, D.; Döblinger, M.; Hettstedt, C.; Karaghiosoff, K.; et al. Synchronized Offset Stacking: A Concept for Growing Large-Domain and Highly Crystalline 2D Covalent Organic Frameworks. *J. Am. Chem. Soc.* **2016**, *138*, 16703–16710. [CrossRef]
30. Ascherl, L.; Sick, T.; Margraf, J.T.; Lapidus, S.H.; Calik, M.; Hettstedt, C.; Karaghiosoff, K.; Döblinger, M.; Clark, T.; Chapman, K.W.; et al. Molecular docking sites designed for the generation of highly crystalline covalent organic frameworks. *Nat. Chem.* **2016**, *8*, 310–316. [CrossRef]
31. Alahakoon, S.B.; Thompson, C.M.; Occhialini, G.; Smaldone, R.A. Design Principles for Covalent Organic Frameworks in Energy Storage Applications. *ChemSusChem* **2017**, *10*, 2116–2129. [CrossRef]
32. Ockwig, N.W.; Chae, H.K.; Eddaoudi, M.; Kim, J.; O'Keeffe, M.; Yaghi, O.M. Reticular synthesis and the design of new materials. *Nature* **2003**, *423*, 705–714. [CrossRef]
33. Cheng, P.; Li, G.; Zhan, X.; Yang, Y. Next-generation organic photovoltaics based on non-fullerene acceptors. *Nat. Photonics* **2018**, *12*, 131–142. [CrossRef]
34. Cheng, P.; Yang, Y. Narrowing the Band Gap: The Key to High-Performance Organic Photovoltaics. *Acc. Chem. Res.* **2020**, *53*, 1218–1228. [CrossRef] [PubMed]
35. Xing, W.; Ye, P.; Lu, J.; Wu, X.; Chen, Y.; Zhu, T.; Peng, A.; Huang, H. Tellurophene-based metal-organic framework nanosheets for high-performance organic solar cells. *J. Power Sources* **2018**, *401*, 13–19. [CrossRef]
36. Zhang, W.; Li, W.; He, X.; Zhao, L.; Chen, H.; Zhang, L.; Tian, P.; Xin, Z.; Fang, W.; Zhang, F. Dendritic Fe-based polyoxometalates @ metal–organic framework (MOFs) combined with ZnO as a novel photoanode in solar cells. *J. Mater. Sci. Mater. Electron.* **2018**, *29*, 1623–1629. [CrossRef]
37. Sasitharan, K.; Bossanyi, D.G.D.G.; Vaenas, N.; Parnell, A.J.A.J.; Clark, J.; Iraqi, A.; Lidzey, D.G.D.G.; Foster, J.A.J.A. Metal-organic framework nanosheets for enhanced performance of organic photovoltaic cells. *J. Mater. Chem. A* **2020**, *8*, 6067–6075. [CrossRef]

38. Bildirir, H.; Gregoriou, V.G.; Avgeropoulos, A.; Scherf, U.; Chochos, C.L. Porous organic polymers as emerging new materials for organic photovoltaic applications: Current status and future challenges. *Mater. Horizons* **2017**, *4*, 546–556. [CrossRef]
39. Su, C.Y.; Dong, Y. Bin Metal-organic frameworks (MOFs). *J. Solid State Chem.* **2015**, *223*, 1. [CrossRef]
40. Yaghi, O.M.; Li, H. Hydrothermal Synthesis of a Metal-Organic Framework Containing Large Rectangular Channels. *J. Am. Chem. Soc.* **1995**, *117*, 10401–10402. [CrossRef]
41. Biondi, C.; Bonamico, M.; Torelli, L.; Vaciago, A. On the structure and water content of copper(II) tricyanomethanide. *Chem. Commun.* **1965**, 191–192. [CrossRef]
42. Hoskins, B.F.; Robson, R. Design and Construction of a New Class of Scaffolding-like Materials Comprising Infinite Polymeric Frameworks of 3D-Linked Molecular Rods. A Reappraisal of the Zn(CN)2 and Cd(CN)2 Structures and the Synthesis and Structure of the Diamond-Related Framework. *J. Am. Chem. Soc.* **1990**, *112*, 1546–1554. [CrossRef]
43. Li, H.; Eddaoudi, M.; O'Keeffe, M.; Yaghi, O.M. Design and synthesis of an exceptionally stable and highly porous metal-organic framework. *Nature* **1999**, *402*, 276–279. [CrossRef]
44. Eddaoudi, M.; Kim, J.; Rosi, N.; Vodak, D.; Wachter, J.; O'Keeffe, M.; Yaghi, O.M. Systematic design of pore size and functionality in isoreticular MOFs and their application in methane storage. *Science* **2002**, *295*, 469–472. [CrossRef] [PubMed]
45. Chae, H.K.; Siberio-Pérez, D.Y.; Kim, J.; Go, Y.B.; Eddaoudi, M.; Matzger, A.J.; O'Keeffe, M.; Yaghi, O.M. A route to high surface area, porosity and inclusion of large molecules in crystals. *Nature* **2004**, *427*, 523–527. [CrossRef] [PubMed]
46. Tao, A.R.; Habas, S.; Yang, P. Shape control of colloidal metal nanocrystals. *Small* **2008**, *4*, 310–325. [CrossRef]
47. Moghadam, P.Z.; Li, A.; Wiggin, S.B.; Tao, A.; Maloney, A.G.P.; Wood, P.A.; Ward, S.C.; Fairen-Jimenez, D. Development of a Cambridge Structural Database Subset: A Collection of Metal-Organic Frameworks for Past, Present, and Future. *Chem. Mater.* **2017**, *29*, 2618–2625. [CrossRef]
48. Furukawa, H.; Cordova, K.E.; O'Keeffe, M.; Yaghi, O.M. The chemistry and applications of metal-organic frameworks. *Science* **2013**, *341*, 1230444. [CrossRef]
49. Fujita, M.; Washizu, S.; Ogura, K.; Kwon, Y.J. Preparation, Clathration Ability, and Catalysis of a Two-Dimensional Square Network Material Composed of Cadmium(II) and 4, 4′-Bipyridine. *J. Am. Chem. Soc.* **1994**, *116*, 1151–1152. [CrossRef]
50. Rosi, N.L.; Eckert, J.; Eddaoudi, M.; Vodak, D.T.; Kim, J.; O'Keeffe, M.; Yaghi, O.M. Hydrogen storage in microporous metal-organic frameworks. *Science* **2003**, *300*, 1127–1129. [CrossRef]
51. Services, R.; Issue, L.; Issues, P.; Service, E.; Links, R.; Blog, C.W.; Newsvine, S.; Products, R. Instant insight: Nothing but surface. *Chem. Soc. Rev.* **2009**, *38*, 12–14. [CrossRef]
52. Vitillo, J.G.; Atzori, C.; Civalleri, B.; Barbero, N.; Barolo, C.; Bonino, F. Design and Characterization of MOFs (Metal–Organic Frameworks) for Innovative Applications. In *Hybrid Organic-Inorganic Interfaces: Towards Advanced Functional Materials*; Delville, M., Taubert, A., Eds.; Wiley-VCH Verlag GmbH & Co. KGaA: Weinheim, Germany, 2017; ISBN 9783527342556.
53. Nasalevich, M.A.; Goesten, M.G.; Savenije, T.J.; Kapteijn, F.; Gascon, J. Enhancing optical absorption of metal-organic frameworks for improved visible light photocatalysis. *Chem. Commun.* **2013**, *49*, 10575–10577. [CrossRef] [PubMed]
54. Stavila, V.; Talin, A.A.; Allendorf, M.D. MOF-based electronic and opto-electronic devices. *Chem. Soc. Rev.* **2014**, *43*, 5994–6010. [CrossRef] [PubMed]
55. Hong, B.J.; Nguyen, S.T.; Hupp, J.T.; Farha, O.K.; Lee, C.Y.; Sarjeant, A.A. Light-Harvesting Metal–Organic Frameworks (MOFs): Efficient Strut-to-Strut Energy Transfer in Bodipy and Porphyrin-Based MOFs. *J. Am. Chem. Soc.* **2011**, *133*, 15858–15861. [CrossRef]
56. Zhang, X.; Ballem, M.A.; Hu, Z.J.; Bergman, P.; Uvdal, K. Nanoscale light-harvesting metal-organic frameworks. *Angew. Chemie Int. Ed.* **2011**, *50*, 5729–5733. [CrossRef]
57. Yan, D.; Tang, Y.; Lin, H.; Wang, D. Tunable two-color luminescence and host-guest energy transfer of fluorescent chromophores encapsulated in metal-organic frameworks. *Sci. Rep.* **2014**, *4*, 4–10. [CrossRef]
58. Kent, C.A.; Mehl, B.P.; Ma, L.; Papanikolas, J.M.; Meyer, T.J.; Lin, W. Energy transfer dynamics in metal-organic frameworks. *J. Am. Chem. Soc.* **2010**, *132*, 12767–12769. [CrossRef]
59. Kreno, L.E.; Leong, K.; Farha, O.K.; Allendorf, M.; Van Duyne, R.P.; Hupp, J.T. Metal-organic framework materials as chemical sensors. *Chem. Rev.* **2012**, *112*, 1105–1125. [CrossRef]

60. Cavka, J.H.; Jakobsen, S.; Olsbye, U.; Guillou, N.; Lamberti, C.; Bordiga, S.; Lillerud, K.P. A new zirconium inorganic building brick forming metal organic frameworks with exceptional stability. *J. Am. Chem. Soc.* **2008**, *130*, 13850–13851. [CrossRef]
61. Morris, W.; Volosskiy, B.; Demir, S.; Gándara, F.; McGrier, P.L.; Furukawa, H.; Cascio, D.; Stoddart, J.F.; Yaghi, O.M. Synthesis, structure, and metalation of two new highly porous zirconium metal-organic frameworks. *Inorg. Chem.* **2012**, *51*, 6443–6445. [CrossRef]
62. Ding, S.Y.; Wang, W. Covalent organic frameworks (COFs): From design to applications. *Chem. Soc. Rev.* **2013**, *42*, 548–568. [CrossRef] [PubMed]
63. Yildirim, O.; Derkus, B. Triazine-based 2D covalent organic frameworks improve the electrochemical performance of enzymatic biosensors. *J. Mater. Sci.* **2020**, *55*, 3034–3044. [CrossRef]
64. Bonomo, M. Synthesis and characterization of NiO nanostructures: A review. *J. Nanoparticle Res.* **2018**, *20*, 222. [CrossRef]
65. Mollamahaleh, Y.B.; Hosseini, D.; Mazaheri, M.; Sadrnezhaad, S.K. Surfactant-Free Production of Ni-Based Nanostructures. *Mater. Sci. Appl.* **2011**, *02*, 444–452. [CrossRef]
66. Demazeau, G. Solvothermal reactions: An original route for the To cite this version: HAL Id: Hal-00269253. *J. Mater. Sci.* **2008**, *7*, 2104–2114. [CrossRef]
67. Zhao, W.; Xia, L.; Liu, X. Covalent organic frameworks (COFs): Perspectives of industrialization. *CrystEngComm* **2018**, *20*, 1613–1634. [CrossRef]
68. Campbell, N.L.; Clowes, R.; Ritchie, L.K.; Cooper, A.I. Rapid Microwave Synthesis and Purification of Porous Covalent Organic Frameworks. *Chem. Mater.* **2009**, *21*, 204–206. [CrossRef]
69. Biswal, B.P.; Chandra, S.; Kandambeth, S.; Lukose, B.; Heine, T.; Banerjee, R. Mechanochemical synthesis of chemically stable isoreticular covalent organic frameworks. *J. Am. Chem. Soc.* **2013**, *135*, 5328–5331. [CrossRef]
70. Yang, C.X.; Liu, C.; Cao, Y.M.; Yan, X.P. Facile room-temperature solution-phase synthesis of a spherical covalent organic framework for high-resolution chromatographic separation. *Chem. Commun.* **2015**, *51*, 12254–12257. [CrossRef]
71. Bella, F.; Gerbaldi, C.; Barolo, C.; Grätzel, M. Aqueous dye-sensitized solar cells. *Chem. Soc. Rev.* **2015**, *44*, 3431–3473. [CrossRef]
72. Barbero, N.; Sauvage, F. Low-cost electricity production from sunlight: Third-generation photovoltaics and the dye-sensitized solar cell. In *Materials for Sustainable Energy Applications: Conversion, Storage, Transmission, and Consumption*; Munoz-Rojas, D., Moya, X., Eds.; Jenny Stanford Publishing: New York, NY, USA, 2016; ISBN 9789814411820.
73. O'Regan, B.; Gratzel, M. A low-cost, high-efficiency solar cell based on dye-sensitized colloidal $TiO_2$ films. *Nature* **1991**, *353*, 737–739. [CrossRef]
74. Nazeeruddin, M.K.; De Angelis, F.; Fantacci, S.; Selloni, A.; Viscardi, G.; Liska, P.; Ito, S.; Takeru, B.; Grätzel, M. Combined experimental and DFT-TDDFT computational study of photoelectrochemical cell ruthenium sensitizers. *J. Am. Chem. Soc.* **2005**, *127*, 16835–16847. [CrossRef]
75. Chen, C.Y.; Wang, M.; Li, J.Y.; Pootrakulchote, N.; Alibabaei, L.; Ngoc-Le, C.H.; Decoppet, J.D.; Tsai, J.H.; Grätzel, C.; Wu, C.G.; et al. Highly efficient light-harvesting ruthenium sensitizer for thin-film dye-sensitized solar cells. *ACS Nano* **2009**, *3*, 3103–3109. [CrossRef] [PubMed]
76. Mathew, S.; Yella, A.; Gao, P.; Humphry-Baker, R.; Curchod, B.F.E.; Ashari-Astani, N.; Tavernelli, I.; Rothlisberger, U.; Nazeeruddin, M.K.; Grätzel, M. Dye-sensitized solar cells with 13% efficiency achieved through the molecular engineering of porphyrin sensitizers. *Nat. Chem.* **2014**, *6*, 242–247. [CrossRef]
77. Kawashima, T.; Ezure, T.; Okada, K.; Matsui, H.; Goto, K.; Tanabe, N. FTO/ITO double-layered transparent conductive oxide for dye-sensitized solar cells. *J. Photochem. Photobiol. A Chem.* **2004**, *164*, 199–202. [CrossRef]
78. Hagfeldt, A.; Boschloo, G.; Sun, L.; Kloo, L.; Pettersson, H. Dye-Sensitized Solar Cells. *Chem. Rev.* **2010**, *110*, 6595–6663. [CrossRef] [PubMed]
79. Bonomo, M.; Dini, D.; Decker, F. Electrochemical and photoelectrochemical properties of nickel oxide (NiO) with nanostructured morphology for photoconversion applications. *Front. Chem.* **2018**, *6*, 601. [CrossRef] [PubMed]
80. Qin, Y.; Peng, Q. Ruthenium Sensitizers and Their Applications in Dye-Sensitized Solar Cells. *Int. J. Photoenergy* **2012**, *2012*, 1–21. [CrossRef]

81. Bella, F.; Bongiovanni, R. Photoinduced polymerization: An innovative, powerful and environmentally friendly technique for the preparation of polymer electrolytes for dye-sensitized solar cells. *J. Photochem. Photobiol. C Photochem. Rev.* **2013**, *16*, 1–21. [CrossRef]
82. Thomas, S.; Deepak, T.G.; Anjusree, G.S.; Arun, T.A.; Nair, S.V.; Nair, A.S. A review on counter electrode materials in dye-sensitized solar cells. *J. Mater. Chem. A* **2014**, *2*, 4474–4490. [CrossRef]
83. Sharma, K.; Sharma, V.; Sharma, S.S. Dye-Sensitized Solar Cells: Fundamentals and Current Status. *Nanoscale Res. Lett.* **2018**, *13*, 381. [CrossRef]
84. Wu, J.; Lan, Z.; Lin, J.; Huang, M.; Huang, Y.; Fan, L.; Luo, G. Electrolytes in Dye-Sensitized Solar Cells. *Chem. Rev.* **2015**, *115*, 2136–2173. [CrossRef]
85. Hardin, B.E.; Snaith, H.J.; McGehee, M.D. The renaissance of dye-sensitized solar cells. *Nat. Photonics* **2012**, *6*, 162–169. [CrossRef]
86. Lee, D.Y.; Shinde, D.V.; Yoon, S.J.; Cho, K.N.; Lee, W.; Shrestha, N.K.; Han, S.H. Cu-based metal-organic frameworks for photovoltaic application. *J. Phys. Chem. C* **2014**, *118*, 16328–16334. [CrossRef]
87. Maza, W.A.; Haring, A.J.; Ahrenholtz, S.R.; Epley, C.C.; Lin, S.Y.; Morris, A.J. Ruthenium(II)-polypyridyl zirconium(IV) metal-organic frameworks as a new class of sensitized solar cells. *Chem. Sci.* **2016**, *7*, 719–727. [CrossRef]
88. Lee, D.Y.; Kim, E.K.; Shin, C.Y.; Shinde, D.V.; Lee, W.; Shrestha, N.K.; Lee, J.K.; Han, S.H. Layer-by-layer deposition and photovoltaic property of Ru-based metal-organic frameworks. *RSC Adv.* **2014**, *4*, 12037–12042. [CrossRef]
89. Liu, J.; Zhou, W.; Liu, J.; Fujimori, Y.; Higashino, T.; Imahori, H.; Jiang, X.; Zhao, J.; Sakurai, T.; Hattori, Y.; et al. A new class of epitaxial porphyrin metal-organic framework thin films with extremely high photocarrier generation efficiency: Promising materials for all-solid-state solar cells. *J. Mater. Chem. A* **2016**, *4*, 12739–12747. [CrossRef]
90. Bella, F.; Bongiovanni, R.; Kumar, R.S.; Kulandainathan, M.A.; Stephan, A.M. Light cured networks containing metal organic frameworks as efficient and durable polymer electrolytes for dye-sensitized solar cells. *J. Mater. Chem. A* **2013**, *1*, 9033–9036. [CrossRef]
91. Lopez, H.A.; Dhakshinamoorthy, A.; Ferrer, B.; Atienzar, P.; Alvaro, M.; Garcia, H. Photochemical response of commercial MOFs: Al2(BDC)3 and its use as active material in photovoltaic devices. *J. Phys. Chem. C* **2011**, *115*, 22200–22206. [CrossRef]
92. Kundu, T.; Sahoo, S.C.; Banerjee, R. Solid-state thermolysis of anion induced metal-organic frameworks to ZnO microparticles with predefined morphologies: Facile synthesis and solar cell studies. *Cryst. Growth Des.* **2012**, *12*, 2572–2578. [CrossRef]
93. Li, Y.; Pang, A.; Wang, C.; Wei, M. Metal-organic frameworks: Promising materials for improving the open circuit voltage of dye-sensitized solar cells. *J. Mater. Chem.* **2011**, *21*, 17259–17264. [CrossRef]
94. Park, J.T.; Moon, J.; Choi, G.H.; Lim, S.M.; Kim, J.H. Facile graft copolymer template synthesis of mesoporous polymeric metal-organic frameworks to produce mesoporous TiO2: Promising platforms for photovoltaic and photocatalytic applications. *J. Ind. Eng. Chem.* **2020**, *84*, 384–392. [CrossRef]
95. Liu, S.; Li, Z.; Zhao, K.; Hao, M.; Zhang, Z.; Li, L.; Zhang, Y.; Zhang, W. A facile hydrothemal synthesis of MoS2@Co3S4 composites based on metal organic framework compounds as a high-efficiency liquid-state solar cell counter electrode. *J. Alloys Compd.* **2020**, *831*, 154910. [CrossRef]
96. Wu, J.; Pan, W.; Lin, Y.Y.; Zhu, J.; Jiang, Q.S.Q.-S.; Zhao, Y.Y.; Ji, R.; Zhang, Y. Metal–organic framework-derived cobalt diselenide as an efficient electrocatalyst for dye-sensitized solar cells. *J. Mater. Sci. Mater. Electron.* **2020**, *31*, 12309–12316. [CrossRef]
97. Padmanathan, S.; Prakasam, A. Incorporation of Carbon Dots on the ZnO Nanosheets as Metal–Organic Framework Photoanodes for High Efficient Dye Sensitized Solar Cell Applications. *J. Clust. Sci.* **2020**, in press. [CrossRef]
98. Gao, J.; Miao, J.; Li, P.Z.; Teng, W.Y.; Yang, L.; Zhao, Y.; Liu, B.; Zhang, Q. A p-type Ti(iv)-based metal-organic framework with visible-light photo-response. *Chem. Commun.* **2014**, *50*, 3786–3788. [CrossRef]
99. Hendon, C.H.; Tiana, D.; Fontecave, M.; Sanchez, C.; D'Arras, L.; Sassoye, C.; Rozes, L.; Mellot-Draznieks, C.; Walsh, A. Engineering the optical response of the titanium-MIL-125 metal-organic framework through ligand functionalization. *J. Am. Chem. Soc.* **2013**, *135*, 10942–10945. [CrossRef]

100. Long, J.; Wang, S.; Ding, Z.; Wang, S.; Zhou, Y.; Huang, L.; Wang, X. Amine-functionalized zirconium metal-organic framework as efficient visible-light photocatalyst for aerobic organic transformations. *Chem. Commun.* **2012**, *48*, 11656–11658. [CrossRef]
101. Sarwar, S.; Lee, M.S.; Park, S.; Dao, T.T.; Ullah, A.; Hong, S.; Han, C.H. Transformation of a liquid electrolyte to a gel inside dye sensitized solar cells for better stability and performance. *Thin Solid Films* **2020**, *704*, 138024. [CrossRef]
102. Oszajca, M.; Podborska, A.; Szaciłowski, K. Unconventional molecular scale logic devices. In *Handbook of Organic Materials for Optical and (Opto)electronic Devices*; Elsevier: Amsterdam, The Netherlands, 2013; ISBN 9780857098764.
103. Jafari, S.; Mahyad, B.; Hashemzadeh, H.; Janfaza, S.; Gholikhani, T.; Tayebi, L. Biomedical applications of $TiO_2$ nanostructures: Recent advances. *Int. J. Nanomedicine* **2020**, *15*, 3447–3470. [CrossRef]
104. Ziental, D.; Czarczynska-Goslinska, B.; Mlynarczyk, D.T.; Glowacka-Sobotta, A.; Stanisz, B.; Goslinski, T.; Sobotta, L. Titanium dioxide nanoparticles: Prospects and applications in medicine. *Nanomaterials* **2020**, *10*, 387. [CrossRef] [PubMed]
105. Dupuy, L.; Haller, S.; Rousset, J.; Donsanti, F.; Guillemoles, J.F.; Lincot, D.; Decker, F. Impedance measurements of nanoporosity in electrodeposited ZnO films for DSSC. *Electrochem. commun.* **2010**, *12*, 697–699. [CrossRef]
106. Minoura, H.; Yoshida, T. Electrodeposition of ZnO/dye hybrid thin films for dye-sensitized solar cells. *Electrochemistry* **2008**, *76*, 109–117. [CrossRef]
107. Turković, A.; Orel, Z.C. Dye-sensitized solar cell with $CeO_2$ and mixed $CeO_2/SnO_2$ photoanodes. *Sol. Energy Mater. Sol. Cells* **1997**, *45*, 275–281. [CrossRef]
108. Zheng, H.; Tachibana, Y.; Kalantar-Zadeh, K. Dye-sensitized solar cells based on $WO_3$. *Langmuir* **2010**, *26*, 19148–19152. [CrossRef]
109. Burnside, S.; Moser, J.-E.; Brooks, K.; Grätzel, M.; Cahen, D. Nanocrystalline mesoporous strontium titanate as photoelectrode material for photosensitized solar devices: Increasing photovoltage through flatband potential engineering. *J. Phys. Chem. B* **1999**, *103*, 9328–9332. [CrossRef]
110. Sayama, K.; Sugihara, H.; Arakawa, H. Photoelectrochemical properties of a porous $Nb_2O_5$ electrode sensitized by a ruthenium dye. *Chem. Mater.* **1998**, *10*, 3825–3832. [CrossRef]
111. Silva, C.G.; Corma, A.; García, H. Metal-organic frameworks as semiconductors. *J. Mater. Chem.* **2010**, *20*, 3141–3156. [CrossRef]
112. Alvaro, M.; Carbonell, E.; Ferrer, B.; Llabrés I Xamena, F.X.; Garcia, H. Semiconductor behavior of a metal-organic framework (MOF). *Chem. A Eur. J.* **2007**, *13*, 5106–5112. [CrossRef] [PubMed]
113. Li, J.; Wan, W.; Zhou, H.; Li, J.; Xu, D. Hydrothermal synthesis of TiO2(B) nanowires with ultrahigh surface area and their fast charging and discharging properties in Li-ion batteries. *Chem. Commun.* **2011**, *47*, 3439–3441. [CrossRef]
114. Jiang, H.L.; Liu, B.; Lan, Y.Q.; Kuratani, K.; Akita, T.; Shioyama, H.; Zong, F.; Xu, Q. From metal-organic framework to nanoporous carbon: Toward a very high surface area and hydrogen uptake. *J. Am. Chem. Soc.* **2011**, *133*, 11854–11857. [CrossRef]
115. Snurr, R.Q.; Wilmer, C.E.; Farha, O.K.; Jeong, N.C.; Yazaydın, A.Ö.; Nguyen, S.T.; Hupp, J.T.; Hauser, B.G.; Sarjeant, A.A.; Eryazici, I. Metal–Organic Framework Materials with Ultrahigh Surface Areas: Is the Sky the Limit? *J. Am. Chem. Soc.* **2012**, *134*, 15016–15021. [CrossRef]
116. Wei, M.; Dou, J.; Li, Y.; Chen, C.; Sun, X. Metal-Organic Frameworks at Interfaces in Dye-Sensitized Solar Cells. *ChemSusChem* **2014**, *7*, 2469–2472. [CrossRef]
117. Joly, F.; Devaux, P.; Loiseau, T.; Arab, M.; Morel, B.; Volkringer, C. Optimization of the synthesis of UiO-66(Zr) in ionic liquids. *Microporous Mesoporous Mater.* **2019**, *288*, 109564. [CrossRef]
118. He, Y.; Zhang, Z.; Wang, W.; Fu, L. Metal organic frameworks derived high-performance photoanodes for DSSCs. *J. Alloys Compd.* **2020**, *825*, 154089. [CrossRef]
119. Chi, W.S.; Roh, D.K.; Lee, C.S.; Kim, J.H. A shape- and morphology-controlled metal organic framework template for high-efficiency solid-state dye-sensitized solar cells. *J. Mater. Chem. A* **2015**, *3*, 21599–21608. [CrossRef]
120. Moad, G.; Jones, R.G.; Alemán, J.V.; Kratochvíl, P.; Stepto, R.F.T.; Hess, M.; Chadwick, A.V.; Penczek, S.; Mita, I.; Horie, K.; et al. Definitions of terms relating to the structure and processing of sols, gels, networks, and inorganic-organic hybrid materials (IUPAC Recommendations 2007). *Pure Appl. Chem.* **2007**, *79*, 1801–1829. [CrossRef]

121. Tao, L.; Huo, Z.; Ding, Y.; Li, Y.; Dai, S.; Wang, L.; Zhu, J.; Pan, X.; Zhang, B.; Yao, J.; et al. High-efficiency and stable quasi-solid-state dye-sensitized solar cell based on low molecular mass organogelator electrolyte. *J. Mater. Chem. A* **2015**, *3*, 2344–2352. [CrossRef]
122. Wang, Y.; Sun, P.; Cong, S.; Zhao, J.; Zou, G. Carbon nanotubes embedding organic ionic plastic crystals electrolytes for high performance solid-state dye-sensitized solar cells. *Carbon N. Y.* **2015**, *92*, 262–270. [CrossRef]
123. Ramasubbu, V.; Kumar, P.R.; Mothi, E.M.; Karuppasamy, K.; Kim, H.S.; Maiyalagan, T.; Shajan, X.S. Highly interconnected porous TiO2-Ni-MOF composite aerogel photoanodes for high power conversion efficiency in quasi-solid dye-sensitized solar cells. *Appl. Surf. Sci.* **2019**, *496*, 143646. [CrossRef]
124. Alwin, S.; Ramasubbu, V.; Sahaya Shajan, X. TiO2 aerogel–metal organic framework nanocomposite: A new class of photoanode material for dye-sensitized solar cell applications. *Bull. Mater. Sci.* **2018**, *41*, 27. [CrossRef]
125. Li, Y.; Che, Z.; Sun, X.; Dou, J.; Wei, M. Metal-organic framework derived hierarchical ZnO parallelepipeds as an efficient scattering layer in dye-sensitized solar cells. *Chem. Commun.* **2014**, *50*, 9769–9772. [CrossRef] [PubMed]
126. Lee, D.Y.; Shin, C.Y.; Yoon, S.J.; Lee, H.Y.; Lee, W.; Shrestha, N.K.; Lee, J.K.; Han, S.H. Enhanced photovoltaic performance of Cu-based metal-organic frameworks sensitized solar cell by addition of carbon nanotubes. *Sci. Rep.* **2014**, *4*, 3930. [CrossRef]
127. Gordillo, M.A.; Panda, D.K.; Saha, S. Efficient MOF-Sensitized Solar Cells Featuring Solvothermally Grown [100]-Oriented Pillared Porphyrin Framework-11 Films on ZnO/FTO Surfaces. *ACS Appl. Mater. Interfaces* **2019**, *11*, 3196–3206. [CrossRef]
128. Khajavian, R.; Ghani, K. Cu-based metal-organic framework thin films: A morphological and photovoltaic study. *J. Solid State Chem.* **2018**, *262*, 94–99. [CrossRef]
129. Carella, A.; Borbone, F.; Centore, R. Research progress on photosensitizers for DSSC. *Front. Chem.* **2018**, *6*, 481. [CrossRef]
130. Shalini, S.; Balasundaraprabhu, R.; Satish Kumar, T.; Prabavathy, N.; Senthilarasu, S.; Prasanna, S. Status and outlook of sensitizers/dyes used in dye sensitized solar cells (DSSC): A review. *Int. J. Energy Res.* **2016**, *40*, 1303–1320. [CrossRef]
131. Saccone, D.; Galliano, S.; Barbero, N.; Quagliotto, P.; Viscardi, G.; Barolo, C. Polymethine Dyes in Hybrid Photovoltaics: Structure-Properties Relationships. *European J. Org. Chem.* **2016**, *2016*, 2244–2259. [CrossRef]
132. Park, J.; Viscardi, G.; Barolo, C.; Barbero, N. Near-infrared sensitization in dye-sensitized solar cells. *Int. J. Chem.* **2013**, *67*, 129–135. [CrossRef]
133. Saygili, Y.; Stojanovic, M.; Flores-Díaz, N.; Zakeeruddin, S.M.; Vlachopoulos, N.; Grätzel, M.; Hagfeldt, A. Metal coordination complexes as redox mediators in regenerative dye-sensitized solar cells. *Inorganics* **2019**, *7*, 30. [CrossRef]
134. Liu, Y.; Jennings, J.R.; Parameswaran, M.; Wang, Q. An organic redox mediator for dye-sensitized solar cells with near unity quantum efficiency. *Energy Environ. Sci.* **2011**, *4*, 564–571. [CrossRef]
135. Hagberg, D.P.; Edvinsson, T.; Marinado, T.; Boschloo, G.; Hagfeldt, A.; Sun, L. A novel organic chromophore for dye-sensitized nanostructured solar cells. *Chem. Commun.* **2006**, 2245–2247. [CrossRef] [PubMed]
136. Mishra, A.; Fischer, M.K.R.; Büuerle, P. Metal-Free organic dyes for dye-Sensitized solar cells: From structure: Property relationships to design rules. *Angew. Chemie Int. Ed.* **2009**, *48*, 2474–2499. [CrossRef]
137. Bonomo, M.; Barbero, N.; Naponiello, G.; Giordano, M.; Dini, D.; Barolo, C. Sodium Hydroxide Pretreatment as an Effective Approach to Reduce the Dye / Holes Recombination Reaction in P-Type DSCs. *Front. Chem.* **2019**, *7*, 1–9. [CrossRef] [PubMed]
138. Liu, J.; Zhou, W.; Liu, J.; Howard, I.; Kilibarda, G.; Schlabach, S.; Coupry, D.; Addicoat, M.; Yoneda, S.; Tsutsui, Y.; et al. Photoinduced Charge-Carrier Generation in Epitaxial MOF Thin Films: High Efficiency as a Result of an Indirect Electronic Band Gap? *Angew. Chemie Int. Ed.* **2015**, *54*, 7441–7445. [CrossRef] [PubMed]
139. Spoerke, E.D.; Small, L.J.; Foster, M.E.; Wheeler, J.; Ullman, A.M.; Stavila, V.; Rodriguez, M.; Allendorf, M.D. MOF-Sensitized Solar Cells Enabled by a Pillared Porphyrin Framework. *J. Phys. Chem. C* **2017**, *121*, 4816–4824. [CrossRef]
140. Joyce, J.T.; Laffir, F.R.; Silien, C. Layer-by-layer growth and photocurrent generation in metal-organic coordination films. *J. Phys. Chem. C* **2013**, *117*, 12502–12509. [CrossRef]
141. Dou, J.; Li, Y.; Xie, F.; Ding, X.; Wei, M. Metal-Organic Framework Derived Hierarchical Porous Anatase TiO2 as a Photoanode for Dye-Sensitized Solar Cell. *Cryst. Growth Des.* **2016**, *16*, 121–125. [CrossRef]

142. Tang, R.; Xie, Z.; Zhou, S.; Zhang, Y.; Yuan, Z.; Zhang, L.; Yin, L. Cu2ZnSnS4 Nanoparticle Sensitized Metal-Organic Framework Derived Mesoporous TiO2 as Photoanodes for High-Performance Dye-Sensitized Solar Cells. *ACS Appl. Mater. Interfaces* **2016**, *8*, 22201–22212. [CrossRef]
143. Du, X.; Fan, R.; Wang, X.; Yu, G.; Qiang, L.; Wang, P.; Gao, S.; Yang, Y. Cooperative Crystallization of Chiral Heterometallic Indium(III)-Potassium(I) Metal-Organic Frameworks as Photosensitizers in Luminescence Sensors and Dye-Sensitized Solar Cells. *Cryst. Growth Des.* **2016**, *16*, 1737–1745. [CrossRef]
144. Meier, S.B.; Tordera, D.; Pertegás, A.; Roldán-Carmona, C.; Ortí, E.; Bolink, H.J. Light-emitting electrochemical cells: Recent progress and future prospects. *Mater. Today* **2014**, *17*, 217–223. [CrossRef]
145. Chen, H.-W.; Lee, J.-H.; Lin, B.-Y.; Chen, S.; Wu, S.-T. Liquid crystal display and organic light-emitting diode display: Present status and future perspectives. *Light Sci. Appl.* **2018**, *7*, 17168. [CrossRef] [PubMed]
146. Babu, H.V.; Bai, M.G.M.; Rajeswara Rao, M. Functional π-Conjugated Two-Dimensional Covalent Organic Frameworks. *ACS Appl. Mater. Interfaces* **2019**, *11*, 11029–11060. [CrossRef] [PubMed]
147. Ahn, D.Y.; Lee, D.Y.; Shin, C.Y.; Bui, H.T.; Shrestha, N.K.; Giebeler, L.; Noh, Y.Y.; Han, S.H. Novel Solid-State Solar Cell Based on Hole-Conducting MOF-Sensitizer Demonstrating Power Conversion Efficiency of 2.1%. *ACS Appl. Mater. Interfaces* **2017**, *9*, 12930–12935. [CrossRef] [PubMed]
148. Kongkanand, A.; Tvrdy, K.; Takechi, K.; Kuno, M.; Kamat, P.V. Quantum dot solar cells. Tuning photoresponse through size and shape control of CdSe-TiO2 architecture. *J. Am. Chem. Soc.* **2008**, *130*, 4007–4015. [CrossRef] [PubMed]
149. Nozik, A.J. Quantum dot solar cells. *Phys. E Low-Dimens. Syst Nanostruct.* **2002**, *14*, 115–120. [CrossRef]
150. Brus, L. Size, dimensionality, and strong electron correlation in Nanoscience. *Acc. Chem. Res.* **2014**, *47*, 2951–2959. [CrossRef] [PubMed]
151. Kamat, P.V. Quantum dot solar cells. The next big thing in photovoltaics. *J. Phys. Chem. Lett.* **2013**, *4*, 908–918. [CrossRef]
152. Farha, O.K.; Wiederrecht, G.P.; Hupp, J.T.; Son, H.-J.; Jin, S. Energy Transfer from Quantum Dots to Metal–Organic Frameworks for Enhanced Light Harvesting. *J. Am. Chem. Soc.* **2013**, *135*, 955–958. [CrossRef]
153. Kaur, R.; Sharma, A.L.; Kim, K.H.; Deep, A. A novel CdTe/Eu-MOF photoanode for application in quantum dot-sensitized solar cell to improve power conversion efficiency. *J. Ind. Eng. Chem.* **2017**, *53*, 77–81. [CrossRef]
154. Kaur, R.; Rana, A.; Singh, R.K.; Chhabra, V.A.; Kim, K.H.; Deep, A. Efficient photocatalytic and photovoltaic applications with nanocomposites between CdTe QDs and an NTU-9 MOF. *RSC Adv.* **2017**, *7*, 29015–29024. [CrossRef]
155. Lin, J.; Nattestad, A.; Yu, H.; Bai, Y.; Wang, L.; Dou, S.X.; Kim, J.H. Highly connected hierarchical textured TiO2 spheres as photoanodes for dye-sensitized solar cells. *J. Mater. Chem. A* **2014**, *2*, 8902–8909. [CrossRef]
156. Lin, J.; Heo, Y.U.; Nattestad, A.; Sun, Z.; Wang, L.; Kim, J.H.; Dou, S.X. 3D hierarchical rutile TiO2 and metal-free organic sensitizer producing dye-sensitized solar cells 8.6% conversion efficiency. *Sci. Rep.* **2014**, *4*, 1–8. [CrossRef] [PubMed]
157. Wang, H.; Hu, Y.H. Graphene as a counter electrode material for dye-sensitized solar cells. *Energy Environ. Sci.* **2012**, *5*, 8182–8188. [CrossRef]
158. Ahmad, I.; McCarthy, J.E.; Bari, M.; Gun'ko, Y.K. Carbon nanomaterial based counter electrodes for dye sensitized solar cells. *Sol. Energy* **2014**, *102*, 152–161. [CrossRef]
159. Park, B.W.; Pazoki, M.; Aitola, K.; Jeong, S.; Johansson, E.M.J.; Hagfeldt, A.; Boschloo, G. Understanding interfacial charge transfer between metallic PEDOT counter electrodes and a cobalt redox shuttle in dye-sensitized solar cells. *ACS Appl. Mater. Interfaces* **2014**, *6*, 2074–2079. [CrossRef]
160. Wang, M.; Anghel, A.M.; Marsan, B.; Ha, N.L.C.; Pootrakulchote, N.; Zakeeruddin, S.M.; Grätzel, M. CoS supersedes Pt as efficient electrocatalyst for triiodide reduction in dye-sensitized solar cells. *J. Am. Chem. Soc.* **2009**, *131*, 15976–15977. [CrossRef] [PubMed]
161. Congiu, M.; Albano, L.G.S.; Decker, F.; Graeff, C.F.O. Single precursor route to efficient cobalt sulphide counter electrodes for dye sensitized solar cells. *Electrochim. Acta* **2015**, *151*, 517–524. [CrossRef]
162. Congiu, M.; Lanuti, A.; di Carlo, A.; Graeff, C.F.O. A novel and large area suitable water-based ink for the deposition of cobalt sulfide films for solar energy conversion with iodine-free electrolytes. *Sol. Energy* **2015**, *122*, 87–96. [CrossRef]
163. Bonomo, M.; Congiu, M.; De Marco, M.L.; Dowling, D.P.; Di Carlo, A.; Graeff, C.F.O.; Dini, D. Limits on the use of cobalt sulfide as anode of p-type dye-sensitized solar cells. *J. Phys. D. Appl. Phys.* **2017**, *50*, 215501. [CrossRef]

164. Hsu, S.H.; Li, C.T.; Chien, H.T.; Salunkhe, R.R.; Suzuki, N.; Yamauchi, Y.; Ho, K.C.; Wu, K.C.W. Platinum-free counter electrode comprised of metal-organic-framework (MOF)-derived cobalt sulfide nanoparticles for efficient dye-sensitized solar cells (DSSCs). *Sci. Rep.* **2014**, *4*, 1–6. [CrossRef] [PubMed]
165. Xia, W.; Zhu, J.; Guo, W.; An, L.; Xia, D.; Zou, R. Well-defined carbon polyhedrons prepared from nano metal-organic frameworks for oxygen reduction. *J. Mater. Chem. A* **2014**, *2*, 11606–11613. [CrossRef]
166. Wang, X.; Xie, Y.; Bateer, B.; Pan, K.; Zhang, X.; Wu, J.; Fu, H. CoSe 2 /N-Doped Carbon Hybrid Derived from ZIF-67 as High-Efficiency Counter Electrode for Dye-Sensitized Solar Cells. *ACS Sustain. Chem. Eng.* **2019**, *7*, 2784–2791. [CrossRef]
167. Ou, J.; Xiang, J.; Liu, J.; Sun, L. Surface-Supported Metal-Organic Framework Thin-Film-Derived Transparent CoS 1.097 @N-Doped Carbon Film as an Efficient Counter Electrode for Bifacial Dye-Sensitized Solar Cells. *ACS Appl. Mater. Interfaces* **2019**, *11*, 14862–14870. [CrossRef]
168. Tian, Y.B.; Wang, Y.Y.; Chen, S.M.; Gu, Z.G.; Zhang, J. Epitaxial Growth of Highly Transparent Metal-Porphyrin Framework Thin Films for Efficient Bifacial Dye-Sensitized Solar Cells. *ACS Appl. Mater. Interfaces* **2020**, *12*, 1078–1083. [CrossRef]
169. Cui, X.; Xie, Z.; Wang, Y. Novel CoS2embedded carbon nanocages by direct sulfurizing metal-organic frameworks for dye-sensitized solar cells. *Nanoscale* **2016**, *8*, 11984–11992. [CrossRef]
170. Lin, Y.; Song, H.; Rao, H.; Du, Z.; Pan, Z.; Zhong, X. MOF-Derived Co,N Codoped Carbon/Ti Mesh Counter Electrode for High-Efficiency Quantum Dot Sensitized Solar Cells. *J. Phys. Chem. Lett.* **2019**, *10*, 4974–4979. [CrossRef]
171. Zhao, L.; Du, J.; Wang, W.; Zhong, X.; Du, Z.; Wang, Y.; Cao, X.-M.; Zhao, L.; Li, Y. Metal–organic framework derived Co,N-bidoped carbons as superior electrode catalysts for quantum dot sensitized solar cells. *J. Mater. Chem. A* **2017**, *6*, 2129–2138. [CrossRef]
172. Kang, J.S.; Kang, J.; Chung, D.Y.; Son, Y.J.; Kim, S.; Kim, S.; Kim, J.; Jeong, J.; Lee, M.J.; Shin, H.; et al. Tailoring the porosity of MOF-derived N-doped carbon electrocatalysts for highly efficient solar energy conversion. *J. Mater. Chem. A* **2018**, *6*, 20170–20183. [CrossRef]
173. Wang, Y.; Yao, M.; Zhao, L.; Wang, W.; Xue, W.; Li, Y. Cu x S nanoparticle@carbon nanorod composites prepared from metal-organic frameworks as efficient electrode catalysts for quantum dot sensitized solar cells. *J. Mater. Chem. A* **2019**, *7*, 2210–2218. [CrossRef]
174. Li, Y.; Liu, X.; Li, H.; Shi, D.; Jiao, Q.; Zhao, Y.; Feng, C.; Bai, X.; Wang, H.; Wu, Q. Rational design of metal organic framework derived hierarchical structural nitrogen doped porous carbon coated CoSe/nitrogen doped carbon nanotubes composites as a robust Pt-free electrocatalyst for dye-sensitized solar cells. *J. Power Sources* **2019**, *422*, 122–130. [CrossRef]
175. Vittal, R.; Chen, T.-Y.; Ho, K.-C.; Li, C.-T.; Kung, C.-W.; Huang, Y.-J. Metal-organic framework/sulfonated polythiophene on carbon cloth as a flexible counter electrode for dye-sensitized solar cells. *Nano Energy* **2016**, *32*, 19–27. [CrossRef]
176. Jiang, X.; Li, H.; Li, S.; Huang, S.; Zhu, C.; Hou, L. Metal-organic framework-derived Ni–Co alloy@carbon microspheres as high-performance counter electrode catalysts for dye-sensitized solar cells. *Chem. Eng. J.* **2018**, *334*, 419–431. [CrossRef]
177. Zhang, W.; Wu, Z.Y.; Jiang, H.L.; Yu, S.H. Nanowire-directed templating synthesis of metal-organic framework nanofibers and their derived porous doped carbon nanofibers for enhanced electrocatalysis. *J. Am. Chem. Soc.* **2014**, *136*, 14385–14388. [CrossRef]
178. Wei, Q.; Xiong, F.; Tan, S.; Huang, L.; Lan, E.H.; Dunn, B.; Mai, L. Porous One-Dimensional Nanomaterials: Design, Fabrication and Applications in Electrochemical Energy Storage. *Adv. Mater.* **2017**, *29*, 1602300. [CrossRef]
179. Park, S.H.; Kim, B.K.; Lee, W.J. Electrospun activated carbon nanofibers with hollow core/highly mesoporous shell structure as counter electrodes for dye-sensitized solar cells. *J. Power Sources* **2013**, *239*, 122–127. [CrossRef]
180. Wan, S.; Guo, J.; Kim, J.; Ihee, H.; Jiang, D. A photoconductive covalent organic framework: Self-condensed arene cubes composed of eclipsed 2D polypyrene sheets for photocurrent generation. *Angew. Chemie Int. Ed.* **2009**, *48*, 5439–5442. [CrossRef]
181. Maitarad, P.; Feng, X.; Guo, J.; Seki, S.; Guo, J.; Nagase, S.; Saeki, A.; Ding, X.; Jiang, D.; Honsho, Y. Synthesis of Metallophthalocyanine Covalent Organic Frameworks That Exhibit High Carrier Mobility and Photoconductivity. *Angew. Chemie Int. Ed.* **2010**, *50*, 1289–1293. [CrossRef]

182. Saeki, A.; Seki, S.; Feng, X.; Nagase, S.; Ding, X.; Honsho, Y.; Jiang, D.; Guo, J.; Chen, L.; Saengsawang, O.; et al. An n-Channel Two-Dimensional Covalent Organic Framework. *J. Am. Chem. Soc.* **2011**, *133*, 14510–14513. [CrossRef]
183. Dong, Y.; Feng, X.; Liu, L.; Saeki, A.; Nagai, A.; Honsho, Y.; Jiang, D.; Irle, S.; Seki, S. High-Rate Charge-Carrier Transport in Porphyrin Covalent Organic Frameworks: Switching from Hole to Electron to Ambipolar Conduction. *Angew. Chemie Int. Ed.* **2012**, *51*, 2618–2622. [CrossRef]
184. Colson, J.W.; Woll, A.R.; Mukherjee, A.; Levendorf, M.P.; Spitler, E.L.; Shields, V.B.; Spencer, M.G.; Park, J.; Dichtel, W.R. Oriented 2D covalent organic framework thin films on single-layer graphene. *Science* **2011**, *332*, 228–231. [CrossRef]
185. Guo, J.; Xu, Y.; Jin, S.; Chen, L.; Kaji, T.; Honsho, Y.; Addicoat, M.A.; Kim, J.; Saeki, A.; Ihee, H.; et al. Conjugated organic framework with three-dimensionally ordered stable structure and delocalized π clouds. *Nat. Commun.* **2013**, *4*, 2736. [CrossRef] [PubMed]
186. Dogru, M.; Handloser, M.; Auras, F.; Kunz, T.; Medina, D.; Hartschuh, A.; Knochel, P.; Bein, T. A photoconductive thienothiophene-based covalent organic framework showing charge transfer towards included fullerene. *Angew. Chemie Int. Ed.* **2013**, *52*, 2920–2924. [CrossRef] [PubMed]
187. Koo, B.T.; Berard, P.G.; Clancy, P. A kinetic monte carlo study of fullerene adsorption within a Pc-PBBA covalent organic framework and implications for electron transport. *J. Chem. Theory Comput.* **2015**, *11*, 1172–1180. [CrossRef]
188. Chen, L.; Furukawa, K.; Gao, J.; Nagai, A.; Nakamura, T.; Dong, Y.; Jiang, D. Photoelectric covalent organic frameworks: Converting open lattices into ordered donor-acceptor heterojunctions. *J. Am. Chem. Soc.* **2014**, *136*, 9806–9809. [CrossRef]
189. Medina, D.D.; Werner, V.; Auras, F.; Tautz, R.; Dogru, M.; Schuster, J.; Linke, S.; Döblinger, M.; Feldmann, J.; Knochel, P.; et al. Oriented thin films of a benzodithiophene covalent organic framework. *ACS Nano* **2014**, *8*, 4042–4052. [CrossRef] [PubMed]
190. Feng, X.; Chen, L.; Honsho, Y.; Saengsawang, O.; Liu, L.; Wang, L.; Saeki, A.; Irle, S.; Seki, S.; Dong, Y.; et al. An ambipolar conducting covalent organic framework with self-sorted and periodic electron donor-acceptor ordering. *Adv. Mater.* **2012**, *24*, 3026–3031. [CrossRef]
191. Jin, S.; Ding, X.; Feng, X.; Supur, M.; Furukawa, K.; Takahashi, S.; Addicoat, M.; El-Khouly, M.E.; Nakamura, T.; Irle, S.; et al. Charge dynamics in a donor-acceptor covalent organic framework with periodically ordered bicontinuous heterojunctions. *Angew. Chemie Int. Ed.* **2013**, *52*, 2017–2021. [CrossRef]
192. Jin, S.; Supur, M.; Addicoat, M.; Furukawa, K.; Chen, L.; Nakamura, T.; Fukuzumi, S.; Irle, S.; Jiang, D. Creation of Superheterojunction Polymers via Direct Polycondensation: Segregated and Bicontinuous Donor-Acceptor π-Columnar Arrays in Covalent Organic Frameworks for Long-Lived Charge Separation. *J. Am. Chem. Soc.* **2015**, *137*, 7817–7827. [CrossRef]
193. Jin, S.; Furukawa, K.; Addicoat, M.; Chen, L.; Takahashi, S.; Irle, S.; Nakamura, T.; Jiang, D. Large pore donor—acceptor covalent organic frameworks. *Chem. Sci.* **2013**, *4*, 4505–4511. [CrossRef]
194. Calik, M.; Auras, F.; Salonen, L.M.; Bader, K.; Grill, I.; Handloser, M.; Medina, D.D.; Dogru, M.; Löbermann, F.; Trauner, D.; et al. Extraction of photogenerated electrons and holes from a covalent organic framework integrated heterojunction. *J. Am. Chem. Soc.* **2014**, *136*, 17802–17807. [CrossRef]
195. You, Y.-M.; Wang, Z.; Niu, X.; Liao, W.-Q.; Zhao, D.; Gao, S.; Ye, H.-Y.; Liu, J.-M.; Fu, D.-W.; Li, J.; et al. An organic-inorganic perovskite ferroelectric with large piezoelectric response. *Science* **2017**, *357*, 306–309. [CrossRef] [PubMed]
196. Zhu, K.; Shrestha, N.; Wang, C.; Podraza, N.J.; Xiao, Y.; Grice, C.R.; Zhao, D.; Yu, Y.; Cimaroli, A.J.; Liao, W.; et al. Fabrication of Efficient Low-Bandgap Perovskite Solar Cells by Combining Formamidinium Tin Iodide with Methylammonium Lead Iodide. *J. Am. Chem. Soc.* **2016**, *138*, 12360–12363. [CrossRef]
197. Liao, W.; Zhao, D.; Yu, Y.; Grice, C.R.; Wang, C.; Cimaroli, A.J.; Schulz, P.; Meng, W.; Zhu, K.; Xiong, R.G.; et al. Lead-Free Inverted Planar Formamidinium Tin Triiodide Perovskite Solar Cells Achieving Power Conversion Efficiencies up to 6.22%. *Adv. Mater.* **2016**, *28*, 9333–9340. [CrossRef] [PubMed]
198. Liao, W.Q.; Zhang, Y.; Hu, C.L.; Mao, J.G.; Ye, H.Y.; Li, P.F.; Huang, S.D.; Xiong, R.G. A lead-halide perovskite molecular ferroelectric semiconductor. *Nat. Commun.* **2015**, *6*, 7338. [CrossRef] [PubMed]
199. Marinova, N.; Valero, S.; Delgado, J.L. Organic and perovskite solar cells: Working principles, materials and interfaces. *J. Colloid Interface Sci.* **2017**, *488*, 373–389. [CrossRef]

200. Bisquert, J.; Garcia-Belmonte, G.; Almora, O.; Jiménez-Tejada, J.A.; Lopez-Varo, P.; García-Rosell, M.; Ravishankar, S. Device Physics of Hybrid Perovskite Solar cells: Theory and Experiment. *Adv. Energy Mater.* **2018**, *8*, 1702772. [CrossRef]
201. Chen, B.; Yang, M.; Priya, S.; Zhu, K. Origin of J-V Hysteresis in Perovskite Solar Cells. *J. Phys. Chem. Lett.* **2016**, *7*, 905–917. [CrossRef]
202. De Wolf, S.; Holovsky, J.; Moon, S.J.; Löper, P.; Niesen, B.; Ledinsky, M.; Haug, F.J.; Yum, J.H.; Ballif, C. Organometallic halide perovskites: Sharp optical absorption edge and its relation to photovoltaic performance. *J. Phys. Chem. Lett.* **2014**, *5*, 1035–1039. [CrossRef]
203. Im, J.H.; Lee, C.R.; Lee, J.W.; Park, S.W.; Park, N.G. 6.5% efficient perovskite quantum-dot-sensitized solar cell. *Nanoscale* **2011**, *3*, 4088–4093. [CrossRef]
204. Ball, J.M.; Lee, M.M.; Hey, A.; Snaith, H.J. Low-temperature processed meso-superstructured to thin-film perovskite solar cells. *Energy Environ. Sci.* **2013**, *6*, 1739–1743. [CrossRef]
205. Kim, H.S.; Im, S.H.; Park, N.G. Organolead halide perovskite: New horizons in solar cell research. *J. Phys. Chem. C* **2014**, *118*, 5615–5625. [CrossRef]
206. You, Y.; Tong, X.; Wang, W.; Sun, J.; Yu, P.; Ji, H.; Niu, X.; Wang, Z.M. Eco-Friendly Colloidal Quantum Dot-Based Luminescent Solar Concentrators. *Adv. Sci.* **2019**, *6*, 1801967. [CrossRef] [PubMed]
207. Chen, B.; Bai, Y.; Yu, Z.; Li, T.; Zheng, X.; Dong, Q.; Shen, L.; Boccard, M.; Gruverman, A.; Holman, Z.; et al. Efficient Semitransparent Perovskite Solar Cells for 23.0%-Efficiency Perovskite/Silicon Four-Terminal Tandem Cells. *Adv. Energy Mater.* **2016**, *6*, 1–7. [CrossRef]
208. Kojima, A.; Teshima, K.; Shirai, Y.; Miyasaka, T. Organometal halide perovskites as visible-light sensitizers for photovoltaic cells. *J. Am. Chem. Soc.* **2009**, *131*, 6050–6051. [CrossRef]
209. Manser, J.S.; Christians, J.A.; Kamat, P.V. Intriguing Optoelectronic Properties of Metal Halide Perovskites. *Chem. Rev.* **2016**, *116*, 12956–13008. [CrossRef]
210. Mariotti, N.; Bonomo, M.; Barolo, C. Emerging photovoltaic technologies and eco-design—Criticisms and potential improvements. In *Criticisms and Potential Improvements, Reliability and Ecological Aspects of Photovoltaic Modules*; Gok, A., Ed.; IntechOpen: London, UK, 2020.
211. Yang, G.; Tao, H.; Qin, P.; Ke, W.; Fang, G. Recent progress in electron transport layers for efficient perovskite solar cells. *J. Mater. Chem. A* **2016**, *4*, 3970–3990. [CrossRef]
212. Nazeeruddin, M.K.; Lee, Y.H.; Bolink, H.J.; Graetzel, M.; Malinkiewicz, O.; Espallargas, G.M.; Yella, A. Perovskite solar cells employing organic charge-transport layers. *Nat. Photonics* **2013**, *8*, 128–132. [CrossRef]
213. Vinogradov, A.V.; Zaake-Hertling, H.; Hey-Hawkins, E.; Agafonov, A.V.; Seisenbaeva, G.A.; Kessler, V.G.; Vinogradov, V.V. The first depleted heterojunction TiO2-MOF-based solar cell. *Chem. Commun.* **2014**, *50*, 10210–10213. [CrossRef]
214. Nguyen, T.M.H.; Bark, C.W. Synthesis of Cobalt-Doped TiO2 Based on Metal-Organic Frameworks as an Effective Electron Transport Material in Perovskite Solar Cells. *ACS Omega* **2020**, *5*, 2280–2286. [CrossRef]
215. Liu, M.; Johnston, M.B.; Snaith, H.J. Efficient planar heterojunction perovskite solar cells by vapour deposition. *Nature* **2013**, *501*, 395–398. [CrossRef] [PubMed]
216. Humphry-Baker, R.; Nazeeruddin, M.K.; Burschka, J.; Gao, P.; Pellet, N.; Grätzel, M.; Moon, S.-J. Sequential deposition as a route to high-performance perovskite-sensitized solar cells. *Nature* **2013**, *499*, 316–319. [CrossRef]
217. Im, J.H.; Jang, I.H.; Pellet, N.; Grätzel, M.; Park, N.G. Growth of CH3 NH3 PbI3 cuboids with controlled size for high-efficiency perovskite solar cells. *Nat. Nanotechnol.* **2014**, *9*, 927–932. [CrossRef] [PubMed]
218. Lindblad, R.; Bi, D.; Park, B.W.; Oscarsson, J.; Gorgoi, M.; Siegbahn, H.; Odelius, M.; Johansson, E.M.J.; Rensmo, H. Electronic structure of TiO2/CH3NH 3PbI3 perovskite solar cell interfaces. *J. Phys. Chem. Lett.* **2014**, *5*, 648–653. [CrossRef]
219. Boopathi, K.M.; Huang, T.-Y.; Chen, H.-W.; Kung, C.-W.; Ho, K.-C.; Kao, S.-Y.; Lu, H.-C.; Chu, C.-W.; Lee, M.-H.; Chang, T.-H. Planar Heterojunction Perovskite Solar Cells Incorporating Metal-Organic Framework Nanocrystals. *Adv. Mater.* **2015**, *27*, 7229–7235. [CrossRef]
220. Kung, C.W.; Chang, T.H.; Chou, L.Y.; Hupp, J.T.; Farha, O.K.; Ho, K.C. Post metalation of solvothermally grown electroactive porphyrin metal-organic framework thin films. *Chem. Commun.* **2015**, *51*, 2414–2417. [CrossRef] [PubMed]
221. Shen, D.; Pang, A.; Li, Y.; Dou, J.; Wei, M. Metal-organic frameworks at interfaces of hybrid perovskite solar cells for enhanced photovoltaic properties. *Chem. Commun.* **2018**, *54*, 1253–1256. [CrossRef] [PubMed]

222. Zhang, Y.-N.; Li, B.; Fu, L.; Li, Q.; Yin, L.-W. MOF-derived ZnO as electron transport layer for improving light harvesting and electron extraction efficiency in perovskite solar cells. *Electrochim. Acta* **2020**, *330*, 135280. [CrossRef]
223. Chen, Z.; Gu, Z.G.; Fu, W.Q.; Wang, F.; Zhang, J. A Confined Fabrication of Perovskite Quantum Dots in Oriented MOF Thin Film. *ACS Appl. Mater. Interfaces* **2016**, *8*, 28737–28742. [CrossRef]
224. Li, M.; Xia, D.; Yang, Y.; Du, X.; Dong, G.; Jiang, A.; Fan, R. Doping of [In2(phen)3Cl6]·CH3CN·2H2O Indium-Based Metal–Organic Framework into Hole Transport Layer for Enhancing Perovskite Solar Cell Efficiencies. *Adv. Energy Mater.* **2018**, *8*, 1702052. [CrossRef]
225. Choi, K.M.; Jeong, H.M.; Park, J.H.; Zhang, Y.B.; Kang, J.K.; Yaghi, O.M. Supercapacitors of nanocrystalline metal-organic frameworks. *ACS Nano* **2014**, *8*, 7451–7457. [CrossRef] [PubMed]
226. Ryu, U.J.; Jee, S.; Park, J.S.; Han, I.K.; Lee, J.H.; Park, M.; Choi, K.M. Nanocrystalline Titanium Metal-Organic Frameworks for Highly Efficient and Flexible Perovskite Solar Cells. *ACS Nano* **2018**, *12*, 4968–4975. [CrossRef] [PubMed]
227. Lee, C.-C.; Chen, C.-I.; Liao, Y.-T.; Wu, K.C.W.; Chueh, C.-C. Enhancing Efficiency and Stability of Photovoltaic Cells by Using Perovskite/Zr-MOF Heterojunction Including Bilayer and Hybrid Structures. *Adv. Sci.* **2019**, *6*, 1801715. [CrossRef] [PubMed]
228. Zhao, X.; Zhao, J.; He, J.; Li, B.; Zhang, Y.; Hu, J.; Wang, H.; Zhang, D.; Liu, Q. Porous Anatase TiO 2 Nanocrystal Derived from the Metal–Organic Framework as Electron Transport Material for Carbon-Based Perovskite Solar Cells. *ACS Appl. Energy Mater.* **2020**, *3*, 6180–6187. [CrossRef]
229. Li, M.; Wang, J.; Jiang, A.; Xia, D.; Du, X.; Dong, Y.; Wang, P.; Fan, R.; Yang, Y. Metal organic framework doped Spiro-OMeTAD with increased conductivity for improving perovskite solar cell performance. *Sol. Energy* **2019**, *188*, 380–385. [CrossRef]
230. Zhou, X.; Qiu, L.; Fan, R.; Wang, A.; Ye, H.; Tian, C.; Hao, S.; Yang, Y. Metal–Organic Framework-Derived N-Rich Porous Carbon as an Auxiliary Additive of Hole Transport Layers for Highly Efficient and Long-Term Stable Perovskite Solar Cells. *Sol. RRL* **2020**, *4*, 1900380. [CrossRef]
231. Seo, S.; Jeong, S.; Bae, C.; Park, N.-G.; Shin, H. Perovskite Solar Cells with Inorganic Electron- and Hole-Transport Layers Exhibiting Long-Term (≈500 h) Stability at 85 °C under Continuous 1 Sun Illumination in Ambient Air. *Adv. Mater.* **2018**, *30*, 1801010. [CrossRef]
232. You, J.; Meng, L.; Song, T.-B.T.B.; Guo, T.F.T.-F.; Chang, W.H.W.-H.; Hong, Z.; Chen, H.; Zhou, H.; Chen, Q.; Liu, Y.; et al. Improved air stability of perovskite solar cells via solution-processed metal oxide transport layers. *Nat. Nanotechnol.* **2016**, *11*, 75–81. [CrossRef]
233. Zhou, X.; Qiu, L.; Fan, R.; Ye, H.; Tian, C.; Hao, S.; Yang, Y. Toward high-efficiency and thermally-stable perovskite solar cells: A novel metal-organic framework with active pyridyl sites replacing 4-tert-butylpyridine. *J. Power Sources* **2020**, *473*, 228556. [CrossRef]
234. Huang, L.; Zhou, X.; Wu, R.; Shi, C.; Xue, R.; Zou, J.; Xu, C.; Zhao, J.; Zeng, W. Oriented haloing metal-organic framework providing high efficiency and high moisture-resistance for perovskite solar cells. *J. Power Sources* **2019**, *433*, 226699. [CrossRef]
235. Dong, Y.; Zhang, J.; Yang, Y.; Qiu, L.; Xia, D.; Lin, K.; Wang, J.; Fan, X.; Fan, R. Self-Assembly of Hybrid Oxidant POM@Cu-BTC for Enhanced Efficiency and Long-Term Stability of Perovskite Solar Cells. *Angew. Chemie Int. Ed.* **2019**, *58*, 17610–17615. [CrossRef] [PubMed]
236. Sardashti, M.K.; Zendehdel, M.; Nia, N.Y.; Karimian, D.; Sheikhi, M. High Efficiency MAPbI3 Perovskite Solar Cell Using a Pure Thin Film of Polyoxometalate as Scaffold Layer. *ChemSusChem* **2017**, *10*, 3773–3779. [CrossRef]
237. Dong, Y.; Yang, Y.; Qiu, L.; Dong, G.; Xia, D.; Liu, X.; Li, M.; Fan, R. Polyoxometalate-Based Inorganic-Organic Hybrid [Cu(phen)2]2[(α-Mo8O26)]: A New Additive to Spiro-OMeTAD for Efficient and Stable Perovskite Solar Cells. *ACS Appl. Energy Mater.* **2019**, *2*, 4224–4233. [CrossRef]
238. Wu, C.; Liu, Y.; Liu, H.; Duan, C.; Pan, Q.; Zhu, J.; Hu, F.; Ma, X.; Jiu, T.; Li, Z.; et al. Highly Conjugated Three-Dimensional Covalent Organic Frameworks Based on Spirobifluorene for Perovskite Solar Cell Enhancement. *J. Am. Chem. Soc.* **2018**, *140*, 10016–10024. [CrossRef] [PubMed]

239. Mohamed, M.G.; Lee, C.C.; EL-Mahdy, A.F.M.; Lüder, J.; Yu, M.H.; Li, Z.; Zhu, Z.; Chueh, C.C.; Kuo, S.W. Exploitation of two-dimensional conjugated covalent organic frameworks based on tetraphenylethylene with bicarbazole and pyrene units and applications in perovskite solar cells. *J. Mater. Chem. A* **2020**, *8*, 11448–11459. [CrossRef]
240. Li, Y.; Chen, Q.; Xu, T.; Xie, Z.; Liu, J.; Yu, X.; Ma, S.; Qin, T.; Chen, L. De Novo Design and Facile Synthesis of 2D Covalent Organic Frameworks: A Two-in-One Strategy. *J. Am. Chem. Soc.* **2019**, *141*, 13822–13828. [CrossRef] [PubMed]